Remote Sensing of Cardiac Activity Based on Signal Reconstruction with Deep Learning

August 2021

Kohei Yamamoto

Remote Sensing of Cardiac Activity Based on Signal Reconstruction with Deep Learning

by

Kohei Yamamoto

Dissertation

Submitted by Kohei Yamamoto

In Partial Fulfillment of the Requirements for the Degree of

Doctor of Philosophy in Engineering

Supervisor: Prof. Tomoaki Otsuki, Ph.D.

Graduate School of Science and Technology
Keio University

August, 2021

Contents

List of Tables

List of Figures

Remote Sensing of Cardiac Activity Based on Signal Reconstruction with Deep Learning

Kohei Yamamoto
ko7243ok@keio.jp.
Keio University, 2021

Supervisor: Prof. Tomoaki Otsuki, Ph.D.
ohtsuki@ics.keio.ac.jp

Abstract

Heartbeat is one of the essential biological signals, and the continuous monitoring of cardiac activity such as the heart rate (HR) enables detecting disease in humans. As a typical method to detect heartbeat, wearable sensors such as Electrocardiogram (ECG) have been used in the past. However, device attachment is sometimes unsuitable for long-term HR monitoring. In contrast, a Doppler radar could be a key device to enable remote sensing of heartbeat without privacy invasion, and various Doppler radar-based heartbeat detection methods have been investigated. However, it is challenging to exploit heartbeat components from received signals of a Doppler radar because the signal-to-noise ratio (SNR) of heartbeat components is lower than those of breathing and body movements.

To deal with this issue, this thesis first proposes a Doppler radar-based heartbeat detection method by using heartbeat signal reconstruction with a deep learning technique, achieving more accurate heartbeat detection. In addition, to obtain more detailed information on cardiac activity, we propose an ECG signal reconstruction method from a Doppler radar signal.

Chapter 1 introduces the background of cardiac activity sensing using a Doppler radar, including some typical methods and these limitations. We also explain the fundamental principle of cardiac activity sensing using a Doppler radar for a better understanding of our proposed methods. We then explain the conventional Doppler radar-based heartbeat detection methods, the motivations and positioning of our research. We then give a brief explanation about the proposed method. We finally describe the contributions of the proposed methods and the outline of this dissertation.

In Chapter 2, we describe related work, including the conventional heartbeat detection methods using a Doppler radar, the existing ECG signal reconstruction methods, and deep learning techniques related to our proposed methods.

In Chapter 3, we present a heartbeat detection method based on heartbeat signal reconstruction with deep learning, for accurate heartbeat detection with robustness to the degradation of the SNR of heartbeat components. Specifically, we first explain the idea of our proposed method, and then we present the proposed algorithm in terms of (i) noise-robust heartbeat component extraction and (ii) heartbeat signal reconstruction based on deep learning. Through the experimental evaluation, we show that our proposed method can detect heartbeat even in the condition where the SNR of heartbeat components is low.

In Chapter 4, we propose an ECG signal reconstruction method based on deep learning via a Doppler radar. We first explain the idea of our proposed method, and then we describe the proposed algorithm based on the results of heartbeat detection. Through some experiments, we show that the proposed method can reconstruct an ECG signal from a Doppler radar signal even without any wearable devices.

Finally, we conclude this dissertation and discuss future work in Chapter 5.

Acknowledgments

Undertaking this PhD has been a truly life-changing experience. It would not have been possible to do without the support, guidance and encouragement of many people.

First and foremost, I would like to express my deepest and sincere gratitude to my supervisor Prof. Tomoaki Ohtsuki for the continuous support and encouragement that he gave me. Without his patience, motivation, and immense knowledge, this PhD would not have been achievable. His advice was crucial to undertake new research challenges and keep persevering even in hard times when results were hard to obtain. I am deeply grateful for all the empowerment I received under his supervision that let me define my own pace.

The committee members Prof. Iwao Sasase, Prof. Masaaki Ikehara, and Prof. Guan Gui, deserve a special mention for their precious time and advice that helped improve the quality of this dissertation.

Assistance provided by Keio Leading Edge Laboratory (KLL) and Center of Innovation Program (COI), by offering grants to support Research during my master and PhD studies has been of great help and deserves a special thank you.

Many Thanks to all the members of Ohtsuki Laboratory, especially Dr. Kentaroh Toyoda, who has always been there for me, has never let me work alone, has always known how to keep me enthusiastic, and has looked forward to facing new challenges. Their unlimited energy is a reference for my future endeavors.

Last but not least, my family and friends gave me great support from both mental and financial aspects. Especially, I would like to express my gratitude to my parents. You all forgave me for proceeding to PhD course without any complaint. Without their support, I could not finish my PhD thesis.

Kohei Yamamoto

Chapter 1

Introduction

This dissertation presents two main topics related to remote sensing of cardiac activity. The first one is heartbeat detection via a Doppler radar. The second one is Electrocardiogram (ECG) signal reconstruction from Doppler radar signal.

1.1 Background

Heartbeat is one of the most critical biological signals to grasp our health condition. Thus, the technique of heartbeat detection has been required in various fields, e.g., the medical field [1][2], the health care field [3][4], and the smart home field [5][6]. As a traditional method to detect the heartbeat, ECG and Photoplethysmography (PPG) have been used broadly.

1.1.1 Cardiac Sensing via ECG

Fig 1.1 shows an example of an ECG sensor. ECG is a device to monitor cardiac activity in detail and has been used widely in the medical field. Fig 1.2 shows an example of an ECG signal. Once the atrial activation starts, a P-wave appears, and subsequently, an R-peak appears due to the ventricular activation. As the ventricle gets relaxed, a T-wave finally appears. The interval between two adjacent R peaks is typically called R-R Interval (RRI), and it is possible to obtain biological information such as heart disease and autonomic activity by monitoring the variability of the RRI and the heart rate (HR). Also, by analyzing the ECG signal, such as the timing of the P-wave, the T-wave, and the R-peak, various heart diseases can be detected [7]-[9].

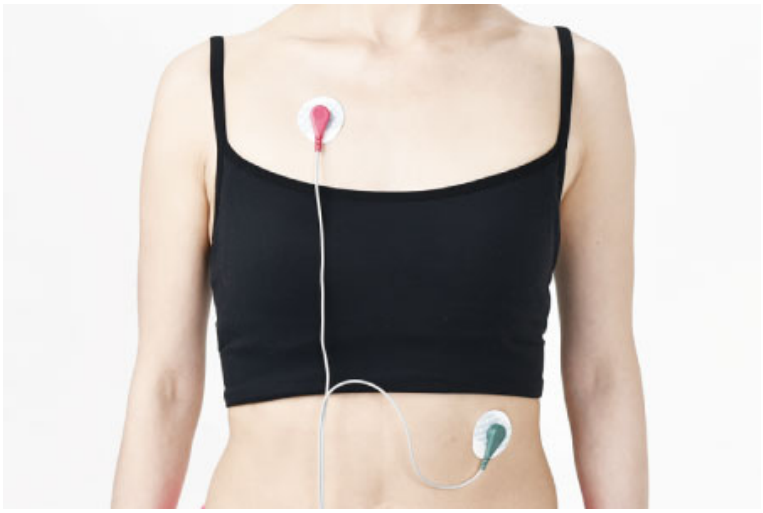

Figure 1.1: ECG sensor. https://www.checkme.jp/ecg/

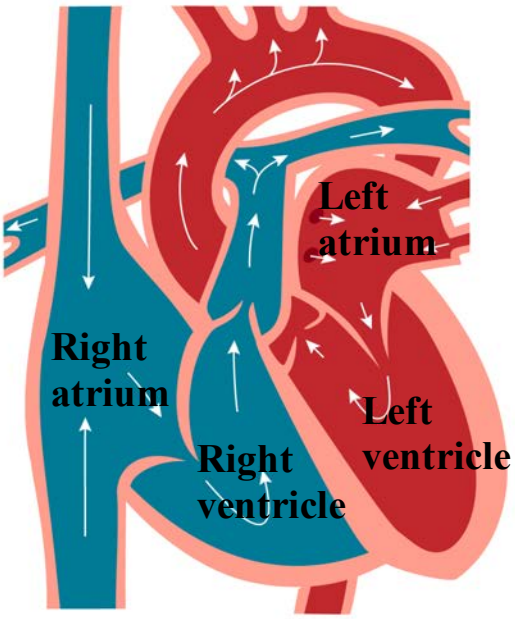

(a) An illustration of a heart.
https://www.ac-illust.com/

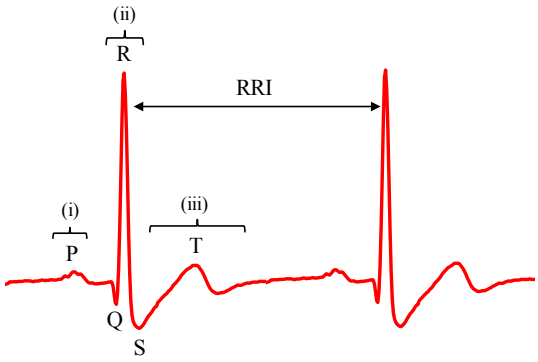

(b) An ECG signal.

Figure 1.2: (a) The illustration of a heart and (b) an ECG signal. (i) A P-wave appears due to the atrial activation, (ii) an R-peak does due to the ventricular activation, and (iii) a T-wave does due to the ventricular relaxation.

1.1.2 Cardiac Sensing via PPG

Fig 1.3 shows an example of an PPG sensor. PPG is also a device that has the potential for heartbeat detection, and it has been mounted on a smartwatch in recent years. PPG emits light on the skin and observes intensity changes of the reflected light. The changes of intensity are caused by heart activity such as heart systole and diastole. By detecting features such as peaks over a PPG signal through some signal processing such as a filter and frequency analysis, it is possible to detect heartbeat.

1.1.3 Advantages and disadvantages of ECG and PPG

Thanks to high-accuracy sensing of heart activity, ECG and PPG have been used in various medical applications, as we mentioned above. In particular, ECG is somewhat robust to noise such as breathing and body fluctuation of a subject his/herself. However, to detect the ECG signal, it is necessary to attach electrodes to a body, and PPG is also a wearable device, which is sometimes unsuitable for some situations, such as long-term monitoring.

1.1.4 Doppler radar

A Doppler radar could be a key device to enable non-contact heartbeat detection. A Doppler radar transmits microwaves toward an object and then receives the microwaves reflected by the object. At the same time when the object reflects the transmitted microwaves, the phase of the microwaves is Doppler-shifted when the object moves. Thus, it is possible to capture the object's motion, such as its velocity and direction, by analyzing the reflected signal. Here, note that the more detailed explanations are given in Chapter 2. Based on this principle, a Doppler radar has been applied in the field such as

- Heartbeat detection [10]-[33]
- Respiration detection [34]-[36]
- Activity recognition [37]-[39]

Figure 1.3: PPG sensor. http://www.svtronics.com/AFE4403-HREVM

In respiration detection, the respiration rate is typically estimated by applying signal processing to a received signal of a Doppler radar. Some researches have focused on respiration pattern recognition [35][36]. In recent years, respiration pattern recognition has been based on machine learning [36]. Also, most of the researches related to activity recognition have investigated to classify abnormal activity, e.g., falling, and normal activity, e.g., walking and sitting. The Doppler-shift is different from one activity to another. Based on this fact, the conventional methods typically extract features from the received signal and then classify activity based on the extracted features with machine learning [37]-[39].

1.2 Cardiac sensing via Doppler radar

In addition to the non-contact feature, the Doppler radar-based heartbeat detection does not require a subject to take off his/her clothing since the microwaves can penetrate the clothing. Also, the cardiac sensing via a Doppler radar does not suffer from the issues related to performance degradation due to the level of brightness and the temperature. Fig. 1.4 shows an example of the Doppler radar used in this research. The size of the radar module for heartbeat detection is not very large, e.g., 12 mm $\times$ 7 mm $\times$ 1 mm of the Doppler radar used in our research. Thus, a

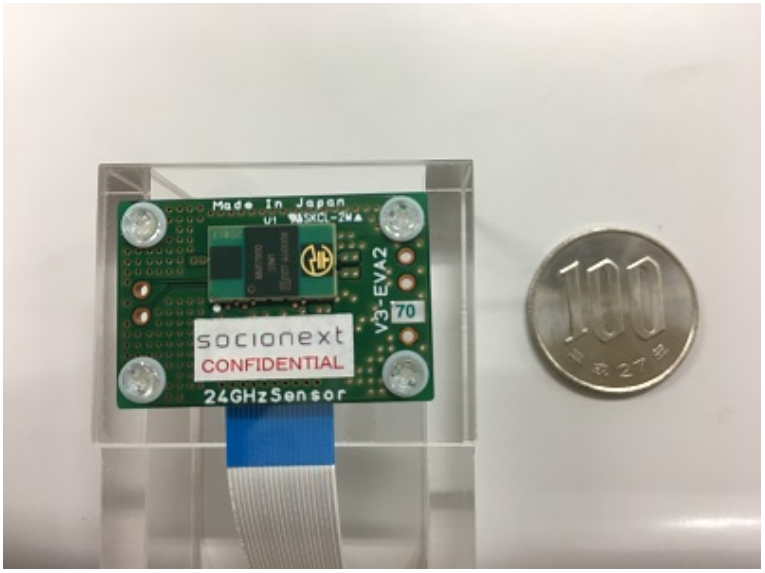

Figure 1.4: An example of the Doppler radar used in this research.

Doppler radar is applicable for heartbeat detection in real applications. Fig. 1.5 shows an example of the application of the Doppler radar-based heartbeat detection: smart home system. This system assumes that it detects humans first and then estimates the location of the human when the human exists. Based on the estimated location, the beam direction of a Doppler radar is adjusted to transmit microwaves toward the human. If the RRI and the HR estimated by Doppler radar-based heartbeat detection are abnormal, the notification representing anomaly will be sent to others. Also, the Doppler radar-based heartbeat detection can be acceptable for those who cannot wear a device. Thus, in addition to such smart home, the Doppler radar-based heartbeat detection can be applied for monitoring a burn patient and an infant who does not prefer device attachment. From a viewpoint of usability, Doppler radar-based heartbeat detection is demanded in these applications, compared to wearable device-based heartbeat detection.

1.2.1 Fundamental principle of cardiac sensing via Doppler radar

In this section, we describe the system model of heartbeat detection with a Doppler radar. The fundamental principle of a Doppler radar is to measure the frequency change caused by the Doppler effect. Fig. 1.6 shows the system model of cardiac sensing with a Doppler radar. Microwaves are transmitted from a Doppler radar toward a subject' chest. When the chest reflects the microwaves, the phase of the microwaves is Doppler-shifted by the chest's displacements due to the subject's

If the RRI and the HR are abnormal, the anomaly notification will be sent to others.

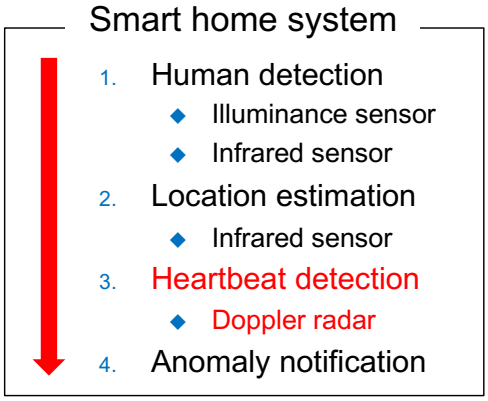

Figure 1.5: An example of the application of the Doppler radar-based heartbeat detection: smart home system. https : //thumb.photo − ac.com/

heartbeat. The Doppler-shift due to the heartbeat, f_{Doppler}, can be expressed as follows.

$$f_{\text{Doppler}} = \pm\frac{4\pi vt}{\lambda} \times \frac{1}{2\pi t} = \pm\frac{2v}{\lambda}, \tag{1.1}$$

where v denotes the speed of the chest displacement. When the chest moves away from the Doppler radar, the minus symbol can be adapted, and vice versa. The Doppler radar then receives the reflected microwaves. The received signal is passed through the low noise amplifier (LNA) and down-converted into the baseband signal $B(t)$. When the chest is a distance d from the Doppler radar, the baseband signal $B(t)$ can be expressed by the wavelength of the carrier λ as the following equation.

$$B(t) = \cos\left(\theta + \frac{4\pi x_h(t)}{\lambda} + \Delta\Phi(t)\right), \tag{1.2}$$

where θ is the constant phase that is dependent on d and the carrier frequency f. Additionally, $x_h(t)$ is the chest displacement caused by the heartbeat, and $\Delta\Phi(t)$ is the total residual phase noise through the circuit and the transmission path. Subsequently, $B(t)$ is demodulated by a quadrature mixer, and two signals, namely, $I(t)$ and $Q(t)$, which are called in-phase and quadrature signals,

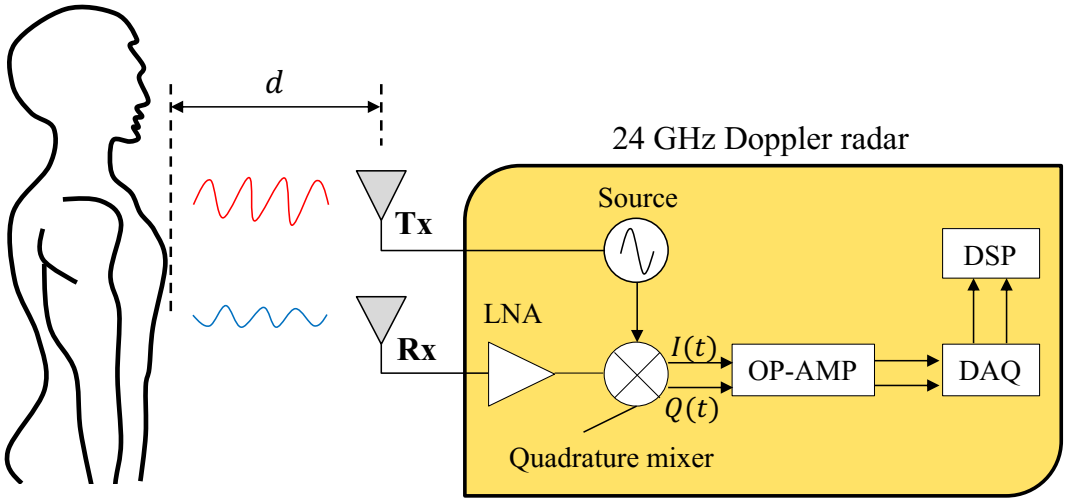

Figure 1.6: The system model of cardiac sensing with a Doppler radar.

respectively, are obtained as follows.

$$I(t) = \cos\left(\theta + \frac{\pi}{4} + \frac{4\pi x_h(t)}{\lambda} + \Delta\Phi(t)\right), \tag{1.3}$$

$$Q(t) = \cos\left(\theta - \frac{\pi}{4} + \frac{4\pi x_h(t)}{\lambda} + \Delta\Phi(t)\right). \tag{1.4}$$

$I(t)$ and $Q(t)$ are then amplified by the operational amplifier (OP-AMP). Fig. 1.7 shows examples of $I(t)$ and $Q(t)$ obtained from a subject sitting still. In this figure, we can see five cycles of the $I(t)$ and $Q(t)$. Each cycle is associated with one breathing. As we can see from this figure, the received signals contains not only heartbeat components but also non-heartbeat components. Therefore, after the data acquisition (DAQ), it is necessary to apply signal processing to the digitized $I(t)$ and $Q(t)$ in the digital signal processing (DSP), for extracting heartbeat components.

To detect heartbeat via a Doppler radar, various Doppler radar-based heartbeat detection methods that analyze a received signal of a Doppler radar have been investigated. Fig. 2.1 shows the summary of the conventional heartbeat detection via a Doppler radar. The Doppler radar-based heartbeat detection methods are typically categorized into two groups: (i) HR estimation [10]-[22] and RRI estimation [23]-[32].

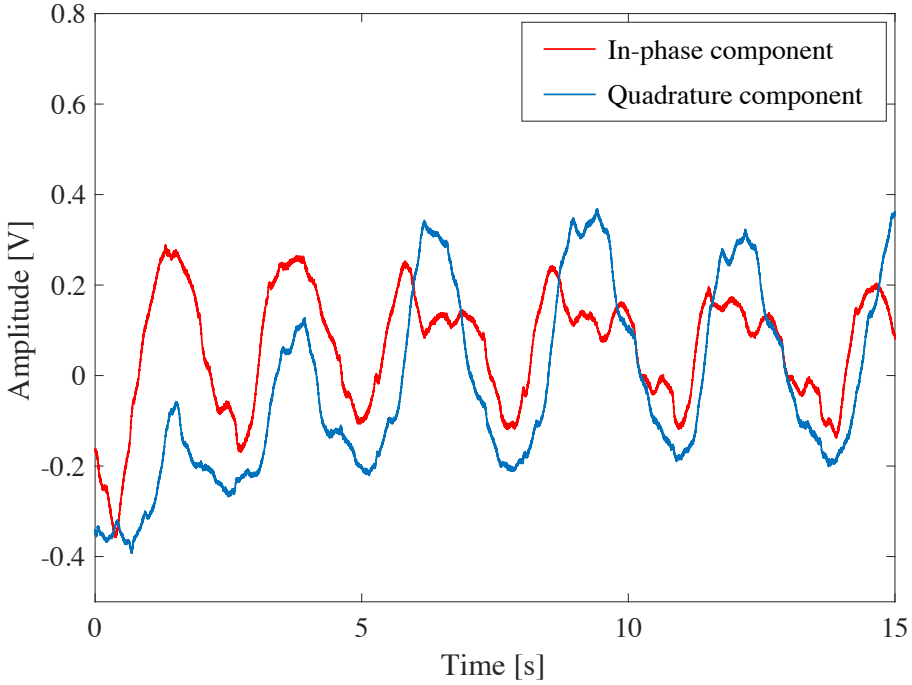

Figure 1.7: Examples of $I(t)$ and $Q(t)$ obtained from a subject sitting still.

1.2.2 HR estimation via Doppler radar

In general, the HR is estimated mainly based on frequency analysis such as

- Fast Fourier Transform (FFT) [10]-[13]
- Wavelet Transform (WT) [14]-[17]
- Multiple Signal Classification (MUSIC) [18]-[21]
- Discrete Cosine Transform (DCT) [22]

Fig. 1.9 shows the typicalHR estimation method with frequency analysis. The HR estimation method prepares a time window, slides the time window by a specific step size, and performs frequency analysis for each time window. To obtain the frequency corresponding to the HR from a received signal of a Doppler radar, it is necessary to set a time window with a frequency resolution that is enough to observe the HR. Thus, the time window longer than 8 s is generally required to achieve a high-frequency resolution. However, the HR could change within the time window and the fast acquisition of the HR is challenging, meaning that it is not possible to track short-term HR changes. Fig. 1.10 shows the HR estimation results of HR estimation methods with

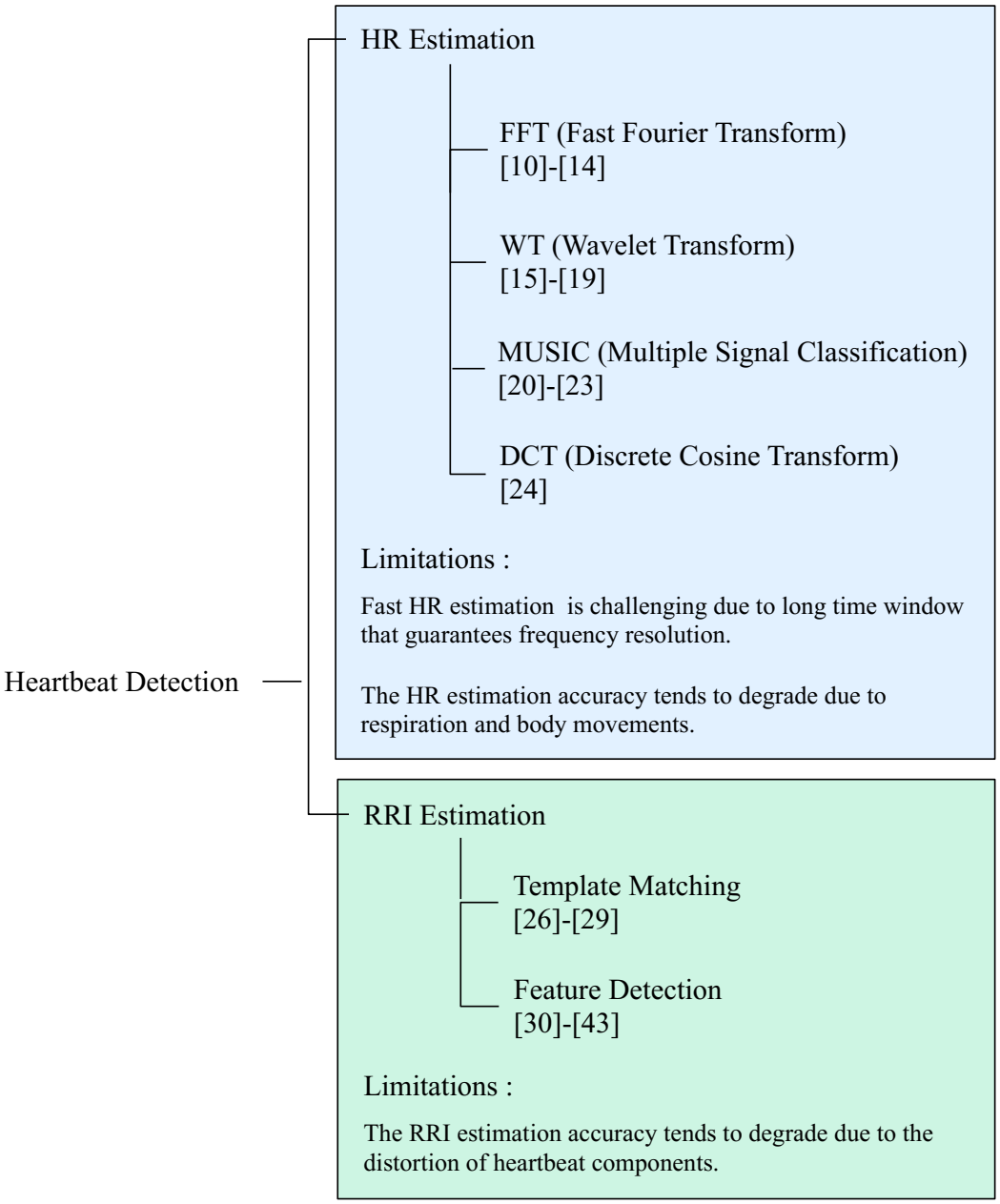

Figure 1.8: The summary of the conventional heartbeat detection methods via a Doppler radar.

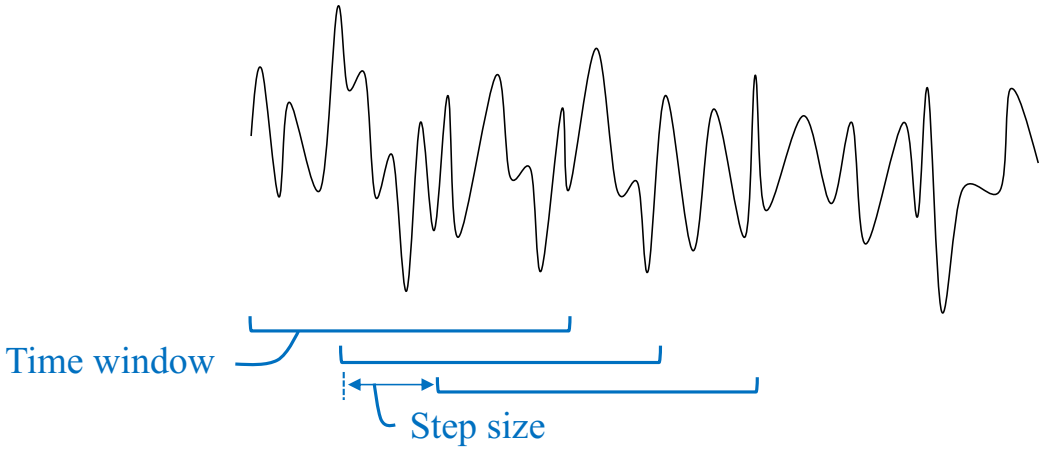

Figure 1.9: The typical HR estimation method with frequency analysis.

different time windows. From this figure, we can see that the method with a long time window does not track short-term HR changes, e.g., around 25 s, while the method with a short time window provides accurate HRs including short-term HR changes. Thus, some researches have attempted to realize the HR estimation methods with a shorter time window [13][17][20]-[22]. However, the conventional HR estimation methods, including the ones with a short time window, suffer from the issues related to performance degradation due to respiration and body movements.

1.2.3 RRI estimation via Doppler radar

The RRI estimation methods can be classified into two group:

- Template matching-based method [24][25]
- Feature extraction-based method [26]-[32]

Fig. 1.11 show the typical RRI estimation method based on (i) template matching algorithm and (ii) feature detection. Some conventional RRI estimation methods prepares a template of a heartbeat signal waveform in advance, and detect heartbeat by comparing the template to the received signal [24][25]. However, the signal-to-noise ratio (SNR) of heartbeat components is low compared to respiration and slight body movements. Therefore, the heartbeat waveform could be easily distorted by such noise, and the heartbeat detection accuracy of template matching-based

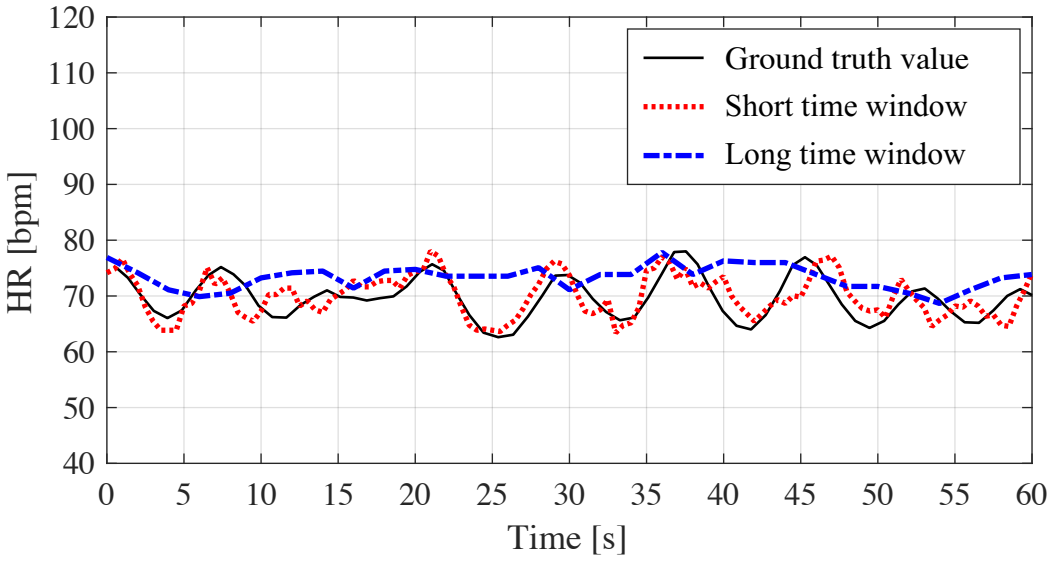

Figure 1.10: The HR estimation results of HR estimation methods with different time windows.

method is likely to degrade. For more accurate RRI estimation, the conventional methods [26]-[32] estimates the RRI by detecting features due to heartbeat, e.g., a peak and zero-crossings, over the signal obtained through some advanced signal processing such as WT and Ensemble Empirical Mode Decomposition (EEMD). Through some experiments, these conventional methods have been shown to provide accurate RRIs in a short-range observation, e.g., a range shorter than 1.0 m. However, as the detection range gets long, the SNR of heartbeat components gets lower [30][33], in general. Thus, for a longer-range observation that is more applicable in real applications, it is still challenging to extract heartbeat components even after signal processing in the conventional methods.

1.2.4 Limitations of conventional heartbeat detection via Doppler radar

As aforementioned, the HR estimation methods have some issues related to fast HR estimation, that is the estimation of short-term HR changes. In addition, the performance of the HR and RRI estimation methods tends to degrade because of respiration and body movements. Furthermore, when the SNR of heartbeat components gets low, the effect of noise components gets higher over a received signal of a Doppler radar, that is, more noise components occur over the received signal.

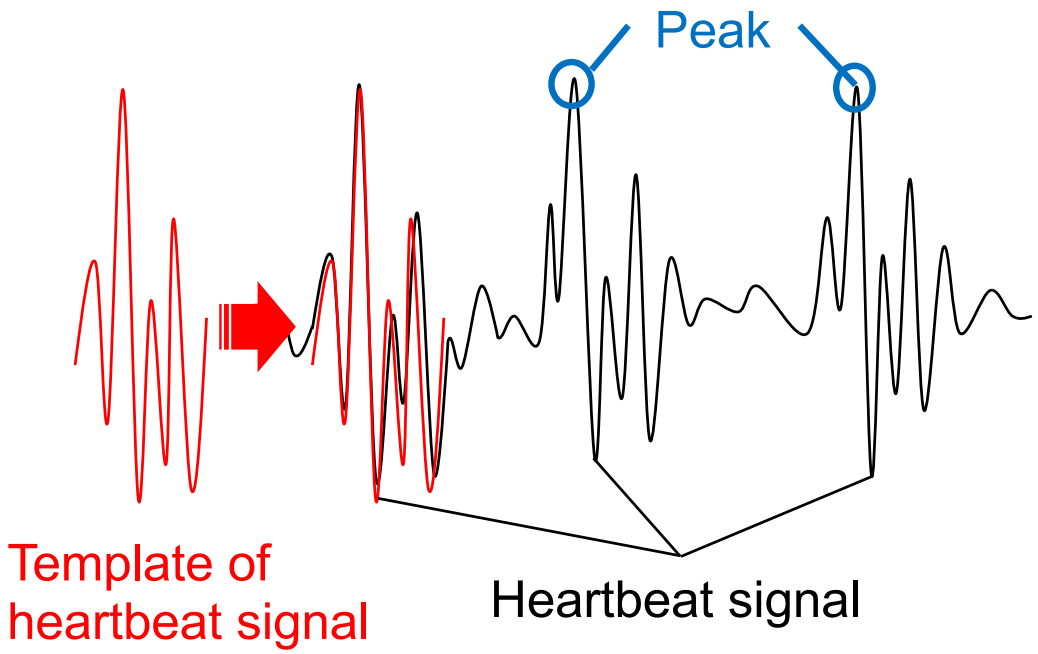

Figure 1.11: The typical RRI estimation method based on (i) template matching algorithm and (ii) feature detection.

Thus, in particular for a subject with low HR, e.g., lower than 50 beat per minute (bpm), the conventional HR estimation methods are likely to estimate the HR higher than the actual HR. In contrast, the conventional RRI estimation methods are likely to estimate the RRI shorter than the actual RRI, in particular for a subject with low HR.

Also, none of the conventional methods have extracted the components corresponding to the P-wave, the T-wave, and the R-peak, though various heart diseases can be identified by analyzing the timings when such waves appear. Detecting the components corresponding to the P-wave and the T-wave is more difficult than detecting the only heartbeat.

1.3 Motivations of our research

From the viewpoint of the limitations of the traditional and the Doppler radar-based cardiac activity sensing methods, we first propose a heartbeat detection method based on heartbeat signal reconstruction with deep learning, for more accurate heartbeat detection. Here, note that our proposed method is a kind of RRI estimation methods, though we show the HR estimation accuracy of

our method through some experiments. The conventional methods estimate the HR and the RRI by signal processing over the frequency-domain, e.g., FFT and MUSIC, and the time-domain, e.g., EEMD and WT. However, these conventional methods are not robust to the degradation of the SNR of heartbeat components. To deal with this issue, we introduce spectrogram-based heartbeat component extraction with more noise-robustness. To further improve the heartbeat detection accuracy against the degradation of the SNR of heartbeat components, we introduce heartbeat signal reconstruction with deep learning based on the extracted heartbeat components. Here, it is worth mentioning that a heartbeat signal represents a signal that heartbeat can be easily detected, e.g., an ECG signal.

We then propose an ECG signal reconstruction method from the Doppler radar-related data for extracting the components corresponding to the P-wave and the T-wave. In contrast to the conventional methods that just estimate the HR and the RRI, we attempt to detect the components corresponding to the P-wave and the T-wave from Doppler radar-related data. The proposed ECG signal reconstruction could expand usage of cardiac activity sensing via a Doppler radar.

1.4 Positioning of our research

Fig. 1.12 shows the types and applications of cardiac activity sensing. Cardiac activity sensing methods can be categorized into wearable device-based and non-contact ones. On the one hand, wearable device-based cardiac activity sensing methods have been mainly realized with ECG, PPG, and Seismocardiogram (SCG). On the other hand, non-contact cardiac activity sensing methods have been mainly investigated with a camera and a Doppler radar. Conventionally, cardiac activity sensing with these devices have realized:

- Blood pressure estimation
- RRI and HR estimation
- ECG signal reconstruction

Blood pressure estimation has been investigated with ECG [55]-[42], PPG [43]-[47] and a Doppler radar [48]-[50]. Also, RRI and HR estimation have been realized with all the devices. ECG signal

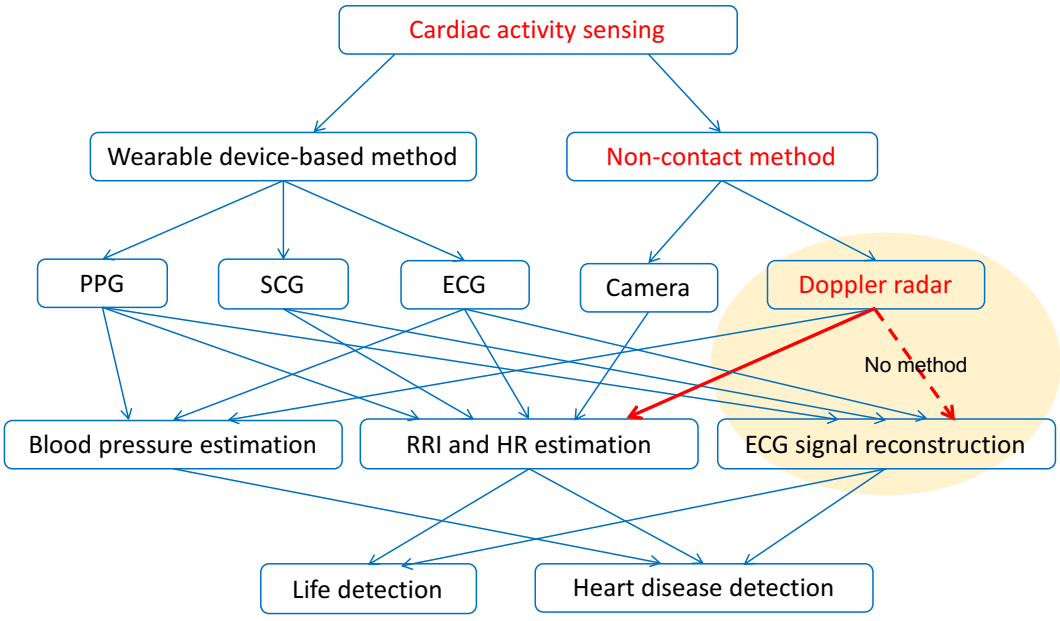

Figure 1.12: The types and applications of cardiac activity sensing.

reconstruction has been realized with PPG [66] and SCG [67]. These three techniques could enable some applications such as life detection and heart disease detection.

In our research, we mainly tackle two targets:

- Doppler radar-based RRI and HR estimation
- Doppler radar-based ECG signal reconstruction

As we mentioned before, RRI and HR estimation using a Doppler radar has been studied extensively in previous researches [10]-[33]. However, there is no conventional methods that exploit the more detailed cardiac activity such as the P-wave and the T-wave from Doppler radar signal.

1.5 Proposed Methods

In this dissertation, we present a heartbeat detection and ECG signal reconstruction methods based on signal reconstruction with deep learning. Fig. 1.13 shows the summary of our proposal. The objective of our proposed heartbeat detection is to extract heartbeat components from a received signal of a Doppler radar, for estimating RRI and HR, which can be done by capturing signal's periodicity. In other words, the proposed heartbeat detection method estimates the timing of each heartbeat. In contrast, the objective of the proposed ECG signal reconstruction is to capture more detailed information on cardiac activity such as a P wave, an R wave, and a T wave, and is different from the objective in the heartbeat detection. The proposed ECG signal reconstruction method estimates an ECG signal corresponding to the Doppler radar signal around the detected heartbeat timing, meaning that one ECG signal is reconstructed one beat by one beat.

1.5.1 Heartbeat detection

Heartbeat component extraction

The conventional heartbeat detection methods mainly use the frequency range from 0.5 Hz to 2.0 Hz corresponding to 30 bpm and 120 bpm to extract heartbeat components. Fig. 1.14 show an example of a received signal corresponding to such frequency. As we can see from this figure, a heartbeat signal with frequency components of 0.5 Hz and 2.0 Hz tends to be distorted by respiration and body movements. This is because the components related to respiration and body

Heartbeat detection	• **Purpose**
	  • Improve the heartbeat detection accuracy against the degradation of the SNR related to heartbeat components
	  • Improve the heartbeat detection accuracy, particularly for the subject with low HR
	• **Heartbeat component extraction**
	  • Based on a spectrogram
	  • With noise-robustness
	• **Heartbeat signal reconstruction**
	  • Based on deep learning
	  • Convolutional LSTM
	  • Reconstruction considering
	  • Periodicity of heartbeat
	  • Spectrum peculiar to just one heartbeat

ECG signal reconstruction	• **Purpose**
	  • Extraction of detailed information on heart activity
	• **Based on CNN and LSTM**
	  • CNN to extract spatial features
	  • LSTM to extract temporal features

Figure 1.13: The summary of our proposal.

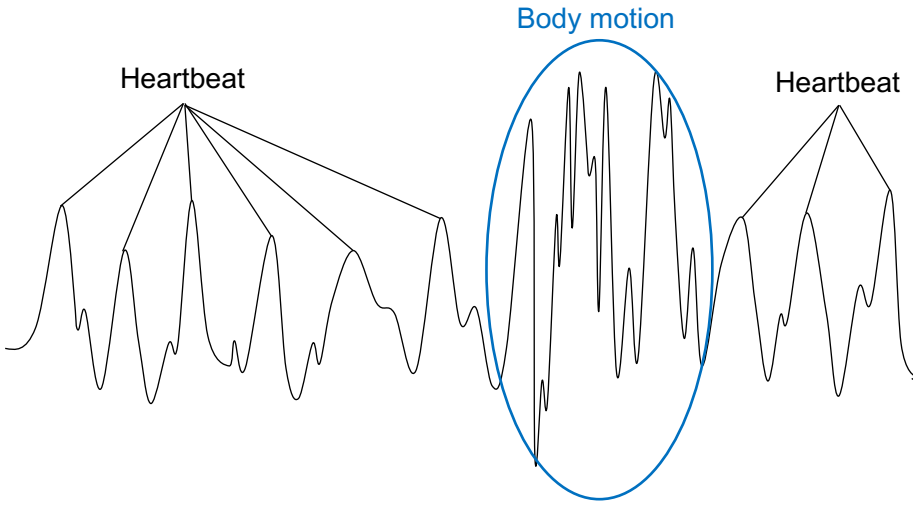

Figure 1.14: An example of a received signal with low-frequency components.

movements are also distributed from 0.5 Hz to 2.0 Hz. The heartbeat detection accuracy is thus likely to degrade over such a frequency range. To reduce the effect of such non-heartbeat components, we first propose a method to extract heartbeat components over a high-frequency range using a spectrogram, compared to the frequency range used in the conventional methods. Unlike the frequency range corresponding to the HR, the high-frequency range contains components due to just one heartbeat. By taking advantage of such a high-frequency range, it is possible to extract heartbeat components with less noise, such as respiration and body movements.

Heartbeat signal reconstruction

Thanks to using the high-frequency range related to just one heartbeat, heartbeat component extraction is more noise-robust. However, when the signal power due to the heartbeat itself gets small, it is more challenging to extract heartbeat components even using the high-frequency range. To further improve the heartbeat detection accuracy, the proposed method reconstructs a heartbeat signal from the spectrogram based on deep learning. The heartbeat components over the spectrogram have two types of features:

- The periodicity of heartbeat, which is peculiar to several heartbeat.

- The spectrum distribution, which is peculiar to one heartbeat.

Inspired by this fact, we use Convolutional Long Short Term Memory (LSTM) as a deep learning model. Convolutional LSTM is one of the deep learning techniques and combines LSTM with the convolutional operation used in Convolutional Neural Network (CNN) [68]. LSTM is a deep learning technique that is useful to extract temporal features of time sequence data [69], and it has been successfully applied to the signal classification [55][56] and prediction [57]. Also, CNN is a deep learning technique that is useful to extract spatial features from image data [73], and it has been successful in image recognition [59]-[61]. The convolutional operation is used in CNN to extract detailed features from image data. Based on the advantages of LSTM and the convolutional operation, convolutional LSTM can extract features from the successive image data. Thus, it is useful for feature extraction for object recognition and frame prediction over movie data [62]-[64]. Based on the above, by inputting the successive spectrograms into convolutional LSTM, it is expected to reconstruct a heartbeat signal well considering the periodicity of heartbeat and the spectrum distribution peculiar to heartbeat.

1.5.2 ECG signal reconstruction

After the heartbeat detection, we introduce an ECG signal reconstruction method to capture the components corresponding to the P-wave and the T-wave from the Doppler radar-related data. As mentioned above, heartbeat components obtained by a Doppler radar tend to be distorted by noise such as respiration and body movements. This means that there exist numerous types of heartbeat signal waveforms. Fig. 1.15 shows an example of a received signal of a Doppler radar. In this figure, the corresponding ECG signal is also shown, and the amplitudes of these two signal are adjusted for a better comparison. As we can see from this figure, the components corresponding to one heartbeat are different from one heartbeat to another, which is mainly due to noise. Therefore, we use deep learning techniques to automatically extract deep features that are useful for the ECG signal reconstruction, even from numerous types of heartbeat signal waveforms. To transform the heartbeat signal to the ECG signal, temporal features of the heartbeat signal are essential. Hence, we use LSTM to extract the temporal features, e.g., the P-wave, the T-wave, and the R-peak appear successively. However, as aforementioned, a heartbeat signal is likely to be deformed due

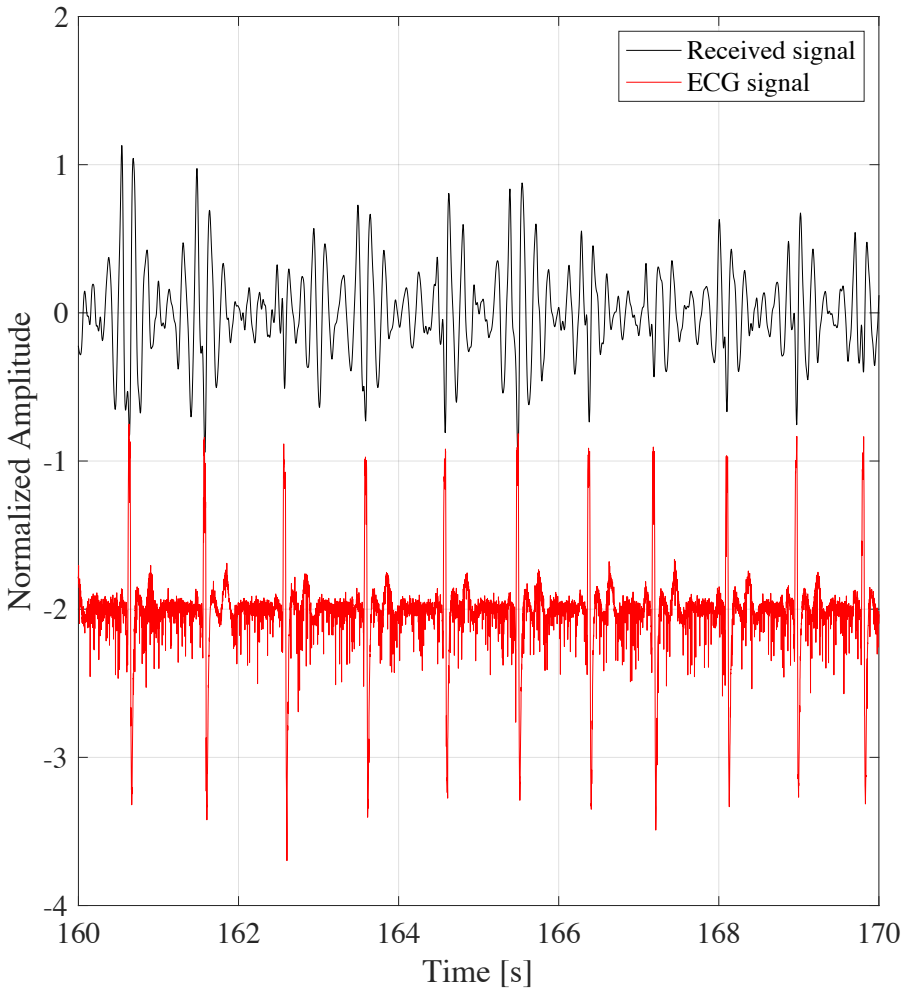

Figure 1.15: Examples of a received signal of a Doppler radar and the corresponding ECG signal.

to noise. To make the model robust to this type of deformation, we first extract spatial features by CNN. After the spatial feature extraction, we extract temporal features by applying LSTM to the output of the CNN. An ECG signal is reconstructed based on the features extracted by the CNN and LSTM. Although the use of only CNN or LSTM might also enable the transformation of the heartbeat signal to the ECG signal, both CNN and LSTM make the model robust against the diversity of the heartbeat signal.

1.6 Contributions of this dissertation

1.6.1 Heartbeat detection in Chapters 3

Figs. 1.16 shows the summary of Chapters 3. This dissertation first introduces a Doppler radar-based heartbeat detection method based on signal reconstruction with deep learning in Chapter 3. In contrast to the most conventional heartbeat detection method using a Doppler radar, the proposed method achieves robust heartbeat detection to the degradation of the SNR of heartbeat components by reconstructing a heartbeat signal based on two features: (i) the periodicity of heartbeat and (ii) the spectrum distribution peculiar to one heartbeat. Through some experiments, we show our proposed method can detect heartbeat in a situation where the distance between a subject and a Doppler radar is long. Also, we show that our proposal has the ability to detect heartbeat, especially for the subjects with low HR, though the heartbeat detection accuracies of the conventional methods tend to degrade for such subjects.

1.6.2 ECG signal reconstruction in Chapter 4

Figs. 1.17 shows the summary of Chapters 4. This dissertation introduces an ECG signal reconstruction method from the Doppler radar-related data in Chapter 4. The proposed method aims to extract detailed heart activity information such as the P-wave and the T-wave of the ECG signal, and our proposal is based on the result of heartbeat detection. Here, it is worth mentioning that none of the conventional Doppler radar-based heartbeat detection methods has realized the extraction of components corresponding to the P-wave and the T-wave. Through some experiments, we show that the proposed method has a good ability to reconstruct an ECG signal. Additionally, we compare our ECG signal reconstruction to the ECG signal reconstruction by attaching devices. We show the feasibility of the non-contact ECG signal reconstruction via a Doppler radar. The experimental results could be a beneficial for expanding usage of cardiac activity sensing with a Doppler radar.

Existing Methods	• **HR estimation method**
	  • FFT（Fast Fourier Transform）
	  • WT（Wavelet Transform）
	  • MUSIC（Multiple Signal Classification）
	  • DCT（Discrete Cosine Transform）
	• **RRI estimation method**
	  • Template matching
	  • Feature detection

Limitations of Existing Methods	• **HR estimation method**
	  • Fast HR estimation is challenging due to long time window that guarantees frequency resolution.
	  • The HR estimation accuracy tends to degrade due to respiration and body movements.
	• **RRI estimation method**
	  • The RRI estimation accuracy tends to degrade due to the distortion of heartbeat components.

Proposed Method	• Spectrogram-based heartbeat extraction • Heartbeat signal reconstruction from spectrogram based on deep learning
Contributions	• The proposed method detects heartbeat more accurately in the situations where the SNR of heartbeat components is low. • The proposed method improves the heartbeat detection accuracy, in particular for the subjects with low HR.

Figure 1.16: The summary of Chapter 3.

Existing Methods	• **PPG-based method** • **SCG-based method** • **None of Doppler radar-based methods**
Limitations of Existing Methods	• PPG and SCG require the device attachment for data collection, which is sometimes undesired in some situations.
Proposed Method	• ECG signal reconstruction based on deep learning from Doppler radar-related data. • The proposed method reconstructs the ECG signal based on the result of heartbeat detection.
Contributions	• The proposed method can reconstruct an ECG signal via a Doppler radar even without device attachment. • Through the performance comparison among our proposed and the existing methods, we show the feasibility of the non-contact ECG signal reconstruction via a Doppler sensor.

Figure 1.17: The summary of Chapter 4.

1.7 Outline of this dissertation

Fig. 1.18 shows the organization of this dissertation. This dissertation consists of five chapters. Chapter 2explains related work on heartbeat detection via a Doppler radar and ECG signal reconstruction, and introduce some deep learning techniques related to our proposed methods. Chapter 3 proposes a novel heartbeat detection method via a Doppler radar. Here, the objective of our proposal is to capture heartbeat from a received signal of a Doppler radar, for estimating RRI and HR, which can be done by capturing signal's periodicity. Chapter 4 present a novel ECG signal reconstruction method via a Doppler radar. The objective of ECG signal reconstruction is to capture more detailed information on cardiac activity such as a P wave, an R wave, and a T wave, and is different from the objective in the heartbeat detection in Chapter 3. Specifically, the timing of each heartbeat is first detected by our proposed heartbeat detection method, and then an ECG signal corresponding to each detected heartbeat is reconstructed based on the Doppler radar signal around the detected timing. These include the description of related work, the algorithm of the proposed method, performance evaluation. Chapter 5 summarizes the overall dissertation and shows our future work.

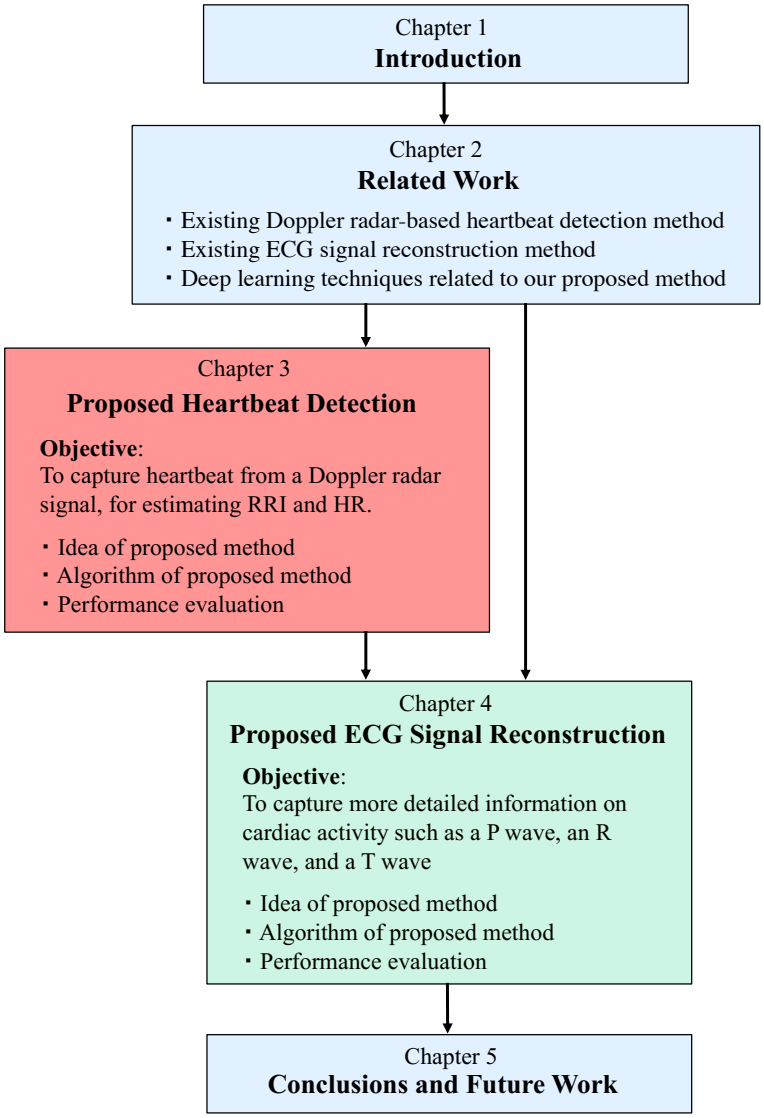

Figure 1.18: The organization of this dissertation

Chapter 2

Related Work

In this chapter, we describe related work. In Section 2.1, we first explain some conventional heartbeat detection methods using a Doppler radar, including our preliminary work, and then explain the shortcomings of the conventional methods. Afterwards, we explain some researches related to ECG signal reconstruction in Section 2.2. For a better understanding of the proposed methods, we introduce some deep learning techniques related to our proposed methods, i.e., LSTM, CNN, and convolutional LSTM in Section 2.3.

2.1 Heartbeat detection via Doppler radar

In this section, we explain previous researches related to Doppler radar-based heartbeat detection. For a better reference, we again show the category and the limitations of the existing heartbeat detection methods in 2.1. In general, the Doppler radar-based heartbeat detection aims at estimating the HR and the RRI.

2.1.1 HR estimation methods using a Doppler radar

On the one hand, the conventional methods estimate the HR leveraging the time-frequency analysis such as

- FFT [10]-[14]
- WT [15]-[19]
- MUSIC [20]-[23]

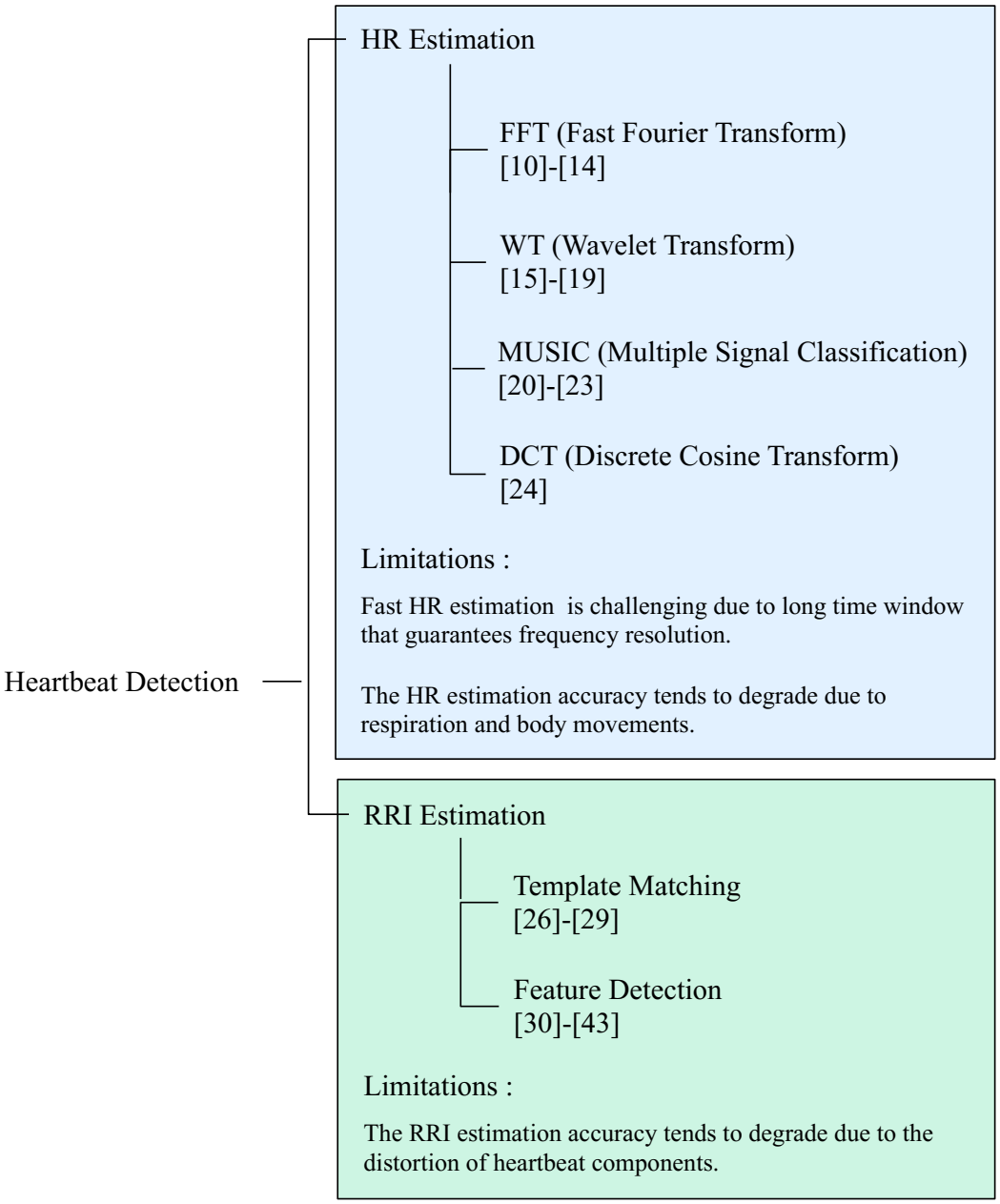

Figure 2.1: The summary of the conventional heartbeat detection methods via a Doppler radar.

- DCT [24]

Tables 2.1, 2.2, 2.3, and 2.4 show the advantages and disadvantages of the conventional FFT, WT, MUSIC, and DCT-based HR estimation methods, respectively. FFT is a typical technique used for analyzing the periodicity of a signal. In general, the normal respiration rate varies between 0.1 Hz and 0.3 Hz, while the normal HR ranges between 0.5 Hz and 2 Hz. Based on this fact, by applying FFT to the received signal of a Doppler radar, the conventional methods separate the frequency components of heartbeat from those of respiration [10]-[12]. However, the SNR of heartbeat components is low, compared to that of respiration. Thus, extracting frequency components of heartbeat could be challenging due to respiration harmonics. The conventional method has introduced a method to reduce the effect of respiration harmonics [13]. However, to estimate the heart rate, a time window longer than 8 s is generally required to achieve a high-frequency resolution. This means that the HR can vary within a time window, and it is impossible to estimate short-term HR changes [10]-[13], e.g., HR changes within 5 s. To deal with this issue, J. Tu *et al.* have proposed HR estimation with a time window shorter than 5 s [14]. However, these conventional methods still have the issue related to the degradation of the HR estimation accuracy due to body movements.

As one of the techniques to analyze the periodicity of a signal, WT has also been used for Doppler radar-based heart rate estimation [15]-[19]. WT analyzes the periodicity of a signal by scaling and shifting the prototype signal called mother wavelet, and provides high time-frequency resolution, compared to FFT. In the WT-based HR estimation method, the HR is estimated by estimating a scale factor. The experimental results have shown that compared to the FFT-based method, the conventional methods [15]-[18] could provide more accurate HR even with a time window shorter than 8 s. However, to estimate short-term HR changes, the time windows used in these conventional methods are long. To address this problem, M. Li *et al.* have proposed a HR estimation method with a shorter time window that is adaptively set [19]. Basically, there are many choices of the prototype signal, and a suitable selection of the prototype signal brings the accurate heart rate estimation. However, non-heartbeat, e.g., respiration and body movements, could deform heartbeat signal waveforms, which changes the suitable prototype signal to estimate the heart rate. Also, a HR estimation accuracy tends to degrade due to body movements.

In addition to FFT and WT, the MUSIC algorithm has also been investigated for the heart rate estimation [20]-[23]. P. Bechet *et al.* have shown the feasibility of the MUSIC algorithm-based heart rate estimation; the MUSIC algorithm provided the accurate heart rate, compared to FFT [20]. However, to estimate the heart rate by the MUSIC algorithm, it is necessary to estimate the number of the sinusoidal signals composing the analyzed signal P. Thus, J. L. Kwang *et al.* have proposed the method that tracks the fundamental and harmonic frequencies of heartbeats over the MUSIC spectrum, and then estimates the heart rate by judging whether at least one of the MUSIC spectrum peaks in the current window appear at the frequencies with the peaks in the previous window [21]. However, this conventional method requires a long time window, i.e., 60 s-time window, so that the MUSIC spectrum peaks appear in such a way even in the presence of the noise. Thus, as aforementioned, it is impossible to estimate the small heart rate variability, e.g., the variability within 5 s. To deal with this problem, the work [22] has proposed a MUSIC algorithm-based heart rate estimation method with a 5 s-time window [15]. The experiment results showed this method achieved the high heart rate estimation accuracy, compared with the conventional one [21]. However, when the heart rate changes largely even within 5 s-time window, several peaks due to heartbeats appear over the MUSIC spectrum, which might cause incorrect peak detection. Such occurrence of several peaks is due to the fixed window size. Thus, in the conventional method [23], the adaptive window size setting technique has been incorporated into the method [22] to prevent such incorrect peak detection. However, there still is an issue related to the degradation of the HR estimation accuracy due to body movements.

Also, the previous research [24] has investigated a HR estimation method based on DCT, which has been used for image compression. Although the conventional method [24] has been shown to achieve a higher HR estimation accuracy even with a short time window than the FFT-based methods, the HR estimation accuracy is likely to degrade due to respiration and body movements. In addition to these HR estimation methods, M. Nosrati *et al.* have introduced the Frequency Time Phase Regression (FTPR) algorithm for the accurate HR estimation [25], compared to the MUSIC-based method. However, this method requires a long time window, i.e., 10 s.

2.1.2 RRI estimation methods using a Doppler radar

On the other hand, in the Doppler radar-based RRI estimation, the RRI can be estimated by

- The template matching algorithm [26]-[29]
- The feature detection [30]-[43]

Tables. 2.5 and 2.6 shows the advantages and disadvantages of the conventional template matching and feature detection-based HR estimation methods, respectively. The template matching-based methods prepare a template waveform of a heartbeat in advance and then detect heartbeats by comparing the received signal with the prepared template waveform [26]-[29]. The conventional methods [26]-[28] could estimate the RRI accurately by using novel peak detection algorithms over the signal obtained through some signal processing. However, the heartbeat signal waveform could change over time, and it is challenging to prepare ideal template waveforms. This is because heartbeat signal waveforms are likely to be distorted by noise such as respiration and body movements. Although the conventional method [29] could estimate the RRI with the robustness to distortion of a heartbeat signal waveform, an RRI estimation accuracy tends to degrade in the situation where the SNR of heartbeat components is low.

In contrast, the feature detection-based RRI estimation method detects heartbeat by extracting features due to a heartbeat from the received signal. Many conventional methods extract peaks from the heartbeat signal waveform as a feature [30]-[36]. These conventional methods could estimate the RRI accurately by using novel peak detection algorithms over the signal obtained through some signal processing, such as a typical filter. However, when the SNR of heartbeat components is low, many incorrect peaks could appear over the signal even after some processing, which could degrade a peak detection accuracy. Furthermore, the conventional methods [37]-[40] could extract a heartbeat signal through some advanced signal processing, e.g., WT and EEMD, which could reduce peak candidates and bring accurate peak detection over the heartbeat signal. Although T. Sakamoto *et al.* have proposed the feature-based correlation method by not only a peak but also extreme points and inflection points of the received signal [40], the heartbeat detection accuracy is likely to degrade as well as the conventional method. Hu *et al.* have proposed the method that estimates the RRI based on zero crossings of the time-domain signal obtained through various signal processing, e.g., WT and EEMD [41]. EEMD can decompose the analyzed signal to some components called IMF (Intrinsic Mode Function) with different frequency components. The conventional method [41] reconstructs a heartbeat signal based on some IMFs, and detects

heartbeat by capturing zero-crossing points of the reconstructed signal. However, it is challenging to select appropriate IMFs for heartbeat signal reconstruction. Also, when the SNR of heartbeat components is low, many incorrect zero-crossing points could appear over the signal even after some processing, which could degrade a zero-crossing detection accuracy. V. L. Petrovic *et al.* have proposed a heartbeat detection method that first estimates a rough HR, designs narrow Band Pass Filter (BPF) with the estimated rough HR as the center frequency. This method then applies the narrow BPF to the signal obtained from a received signal of a Doppler radar and detects heartbeat by the zero-crossings of the selected BPF output [42]. Although the experimental results show that this method can provide an accurate heartbeat detection accuracy as long as the SNR of heartbeat components is high, it is still challenging to detect heartbeat accurately with robustness to low SNR.

Table 2.1: The advantages and disadvantages of the conventional FFT-based HR estimation methods.

Method	Advantages	Disadvantages
[10][11][12]	♦ The methods could separate frequency components of heartbeat from those of respiration over the FFT spectrum.	♦ The methods require a long-time window for achieving a high-frequency resolution. ♦ Several peaks corresponding to the HR could appear over the FFT spectrum, which could bring incorrect peak detection. ♦ The HR estimation accuracy tends to degrade due to respiration and body movements.
[13]	♦ The method suppresses the effect of respiration harmonics.	♦ The methods require a long-time window for achieving a high-frequency resolution. ♦ Several peaks corresponding to the HR could appear over the FFT spectrum, which could bring incorrect peak detection. ♦ The HR estimation accuracy tends to degrade due to body movements.
[14]	♦ The method estimates the HR with a short time window and suppresses the effect of respiration harmonics	♦ A HR estimation accuracy tends to degrade due to body movements.

Table 2.2: The advantages and disadvantages of the conventional WT-based HR estimation methods.

Method	Advantages	Disadvantages
[15][16] [17][18]	♦ The methods could provide more accurate HR than the FFT-based methods. ♦ Compared to the FFT-based method, the methods could estimate the HR with a short time window, e.g., shorter than 8 s.	♦ Appropriate prototype signals can change over time, because a heartbeat signal tends to be distorted by respiration and body movements. ♦ The HR estimation accuracy tends to degrade due to respiration and body movements.
[19]	♦ The method could provide more accurate HR than the FFT-based methods. ♦ The method realizes fast HR estimation, i.e., with a time window shorter than 5 s. ♦ The method suppresses the effect of respiration harmonics.	♦ The HR estimation accuracy tends to degrade due to body movements.

Table 2.3: The advantages and disadvantages of the conventional MUSIC-based HR estimation methods.

Method	Advantages	Disadvantages
[20]	♦ The method could provide more accurate HR than the FFT-based methods.	♦ The HR estimation accuracy depends on the parameter *P*. ♦ Several peaks corresponding to the HR could appear over the MUSIC spectrum, which could bring incorrect peak detection.
[21]	♦ The method could provide more accurate HR than the FFT-based methods. ♦ The method can estimate the HR without parameter *P*.	♦ The method requires a long-time window, e.g., 60 s. ♦ Several peaks corresponding to the HR could appear over the MUSIC spectrum, which could bring incorrect peak detection.
[22]	♦ The method realizes fast HR estimation, i.e., with a time window shorter than 5 s. ♦ The HR estimation accuracy does not depend on parameter *P*.	♦ Several peaks corresponding to the HR could appear over the MUSIC spectrum, which could bring incorrect peak detection. ♦ The HR estimation accuracy tends to degrade due to body movements.
[23]	♦ The method realizes fast HR estimation, i.e., with a time window shorter than 5 s. ♦ The HR estimation accuracy does not depend on parameter *P*. ♦ The method could prevent wrong peak detection due to several peaks corresponding to the HR.	♦ The HR estimation accuracy tends to degrade due to respiration and body movements.

Table 2.4: The advantages and disadvantages of the conventional DCT-based HR estimation method.

Method	Advantages	Disadvantages
[24]	♦ The methods could provide more accurate HR than the FFT-based methods. ♦ The method realizes fast HR estimation, i.e., with a time window shorter than 5	♦ The HR estimation accuracy tends to degrade due to respiration and body movements.

Table 2.5: The advantages and disadvantages of the conventional template matching-based RRI estimation methods.

Method	Advantages	Disadvantages
[26][27][28]	♦ The methods could estimate the RRI with a template of a heartbeat signal waveform in the situation where the SNR of heartbeat components is high.	♦ Heartbeat signal waveforms tend to be distorted by respiration and body movements, which degrade a heartbeat detection accuracy.
[29]	♦ The method could estimate the RRI with the robustness to distortion of a heartbeat signal waveform.	♦ In the situation where the SNR of heartbeat components is low, an RRI estimation accuracy tends to degrade.

Table 2.6: The advantages and disadvantages of the conventional feature detection-based RRI estimation methods.

Method	Advantages	Disadvantages
[30]-[36]	♦ The methods could estimate the RRI accurately by using novel peak detection algorithm over the signal obtained through some signal processing.	♦ In the situation where the SNR of heartbeat components is low, many incorrect peaks could appear over the signal even after some processing, which could degrade a peak detection accuracy.
[37]-[40]	♦ The methods could extract a heartbeat signal through some advanced signal processing, e.g., WT and EEMD, which could bring accurate peak detection over the heartbeat signal.	♦ In the situation where the SNR of heartbeat components is low, many incorrect peaks could appear over the signal even after some processing, which could degrade a peak detection accuracy.
[41]	♦ The method could estimate the RRI by extracting not only peaks but also other features peculiar to heartbeat, e.g., inflection points.	♦ Heartbeat signal waveforms tend to be distorted by respiration and body movements, which could degrade a feature detection accuracy.
[42][43]	♦ The methods could extract a heartbeat signal through some advanced signal processing, e.g., WT and EEMD. ♦ The methods which could estimate the RRI accurately by detecting zero-crossing points.	♦ In the situation where the SNR of heartbeat components is low, many incorrect zero-crossing points could appear over the signal even after some processing, which could degrade a zero-crossing detection accuracy.

2.1.3 Our preliminary research

In our preliminary research [43], to accurately pick up peaks due to heartbeat, we have investigated the peak selection algorithm considering several peaks just before and after the investigated peaks. Algorithm 1 shows the RRI estimation algorithm by the peak detection. In our peak detection, BPF is firstly applied to the analyzed signal to reduce the effect of the undesired peaks. The way to set its cut-off frequencies f_{L2} and f_{U2} is explained later. After filtering, the peaks due to heartbeats are detected using some peaks before and after the investigated peak. Fig. 2.2 shows a concept of the proposed peak detection algorithm. In what follows, we explain how our peak detection algorithm works with this figure. Although eight peaks are observed in total within a time window in Fig. 2.2, some of them are related to heartbeats while others are due to noise. So it is necessary to choose only heartbeat peaks. Three peaks, p_1, p_2 and p_3 ($p_1 < p_2 < p_3$) are out of the peaks 1, 2, ..., and 8 so that the difference among the previously estimated RRI RRI_{prev} and two pairs of RRI candidates is the smallest. This is because the RRI does not largely vary between the adjacent RRIs in general. Here, we denote $RRI_{i,j}$ as the RRI in between peaks i and j, where $1 \leq i \leq 8$ and $1 \leq j \leq 8$. In Fig. 2.2, assuming that RRI_{prev} is estimated correctly, the peak 1 is chosen as p_1. The pairs of $RRI_{1,k}$ ($2 < k < 8$) and $RRI_{k,m}$ ($k < m < 8$) are then generated, e.g., $RRI_{1,2}$ and $RRI_{2,5}$. As p_1, p_2 and p_3 that meet the condition where the difference among RRI_{prev}, $RRI_{1,k}$ and $RRI_{k,m}$ is the smallest, the peaks 1, 3, and 5 are finally chosen. Based on the fact that the RRI typically does not change largely between the adjacent RRIs, a time window is set using the previously estimated RRI RRI_{prev}. Now, let Δ be the maximum difference between the current and previous RRI. When RRI increases by Δ twice in a row, the current RRI RRI_{curr} is equal to $RRI_{\mathrm{prev}} + \Delta$, and then the next RRI is equal to $RRI_{\mathrm{curr}} + \Delta$, i.e., $RRI_{\mathrm{prev}} + 2\Delta$ as shown in Fig. 2.2. Therefore, the length of a time window W is set as the following equation so that the window includes just three heartbeats.

$$W = 2RRI_{\mathrm{prev}} + 3\Delta, \tag{2.1}$$

where Δ is set as 150 ms in our method. In the initial observation where RRI_{prev} is not still estimated, the peaks due to heartbeats are detected by a simple peak detection for several seconds, including two or three heartbeats. On the other hand, when the RRI decreases by Δ twice in a row,

Algorithm 1 RRI estimation algorithm by the peak detection

Require: $p3 > p2 > p1$
Input: $Sig(t)$: the analyzed signal
1: **function** RRI_ESTIMATOR($Sig(t)$, W, $prevRRI$, f_{L2}, f_{U2})
2: Apply BPF with its cut-off frequencies f_{L2} and f_{U2} to $Sig(t)$
3: Generate some pairs of the RRI candidates within the time window with its size W
4: Find three peaks, $p1$, $p2$ and $p3$, so that the difference among two RRI candidates paired and RRI_{prev} is the smallest.
5: Estimate RRI based on $p1$ and $p2$
6: $prevRRI \Leftarrow RRI$
7: PARAMETWR_TUNER(RRI_{prev}, Δ);
8: **end function**
9: **function** PARAMETER_TUNER(RRI_{prev}, Δ)
10: $W \Leftarrow 2RRI_{\mathrm{prev}} + 3\Delta$
11: $overlap \Leftarrow RRI_{\mathrm{prev}}$
12: $f_{\mathrm{L2}} \Leftarrow \frac{1}{RRI_{\mathrm{prev}}+\Delta}$
13: $f_{\mathrm{U2}} \Leftarrow \frac{1}{RRI_{\mathrm{prev}}-\Delta}$
14: **end function**

the time window includes three or four heartbeats depending on RRI_{prev}. For each window set in this way, only one RRI is estimated based on the peaks $pks1$ and $pks2$ in our method. RRI_{prev} is updated to the estimated RRI, i.e., $RRI_{1,3}$. The time window with the length W slides by RRI_{prev}.The overlap of a time window is then set as RRI_{prev}. Furthermore, since the maximum difference between the current and previous RRI is determined as Δ, the cut-off frequencies f_{L2} and f_{U2} are set using RRI_{prev} and Δ as the following equations, which results in the reduction of the number of the peaks due to non-heartbeats.

$$f_{\mathrm{L2}} = \frac{1}{RRI_{\mathrm{prev}} + \Delta}, \tag{2.2}$$

$$f_{\mathrm{U2}} = \frac{1}{RRI_{\mathrm{prev}} - \Delta}. \tag{2.3}$$

In the initial observation, f_{L2} and f_{U2} are initialized to be 0.5 Hz and 2 Hz corresponding to 30 bpm and 120 bpm, respectively.

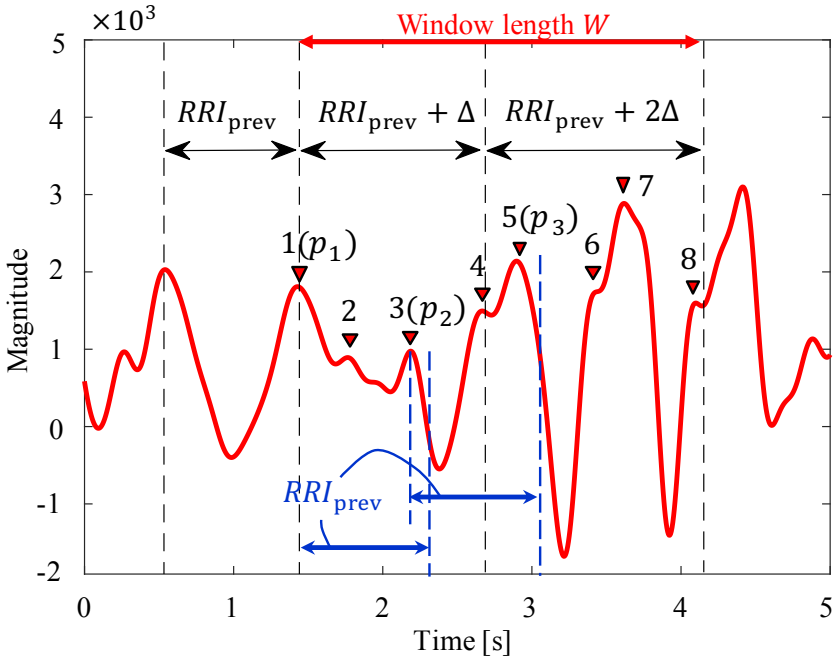

Figure 2.2: A concept of the proposed peak detection algorithm.

2.1.4 Main issues of conventional heartbeat detection methods

Although these conventional heartbeat detection methods, including our previous method [43], have been experimentally shown to be able to detect heartbeat, the heartbeat detection accuracy could get degraded due to respiration and slight body movements. This is because compared to respiration and slight body movements, the SNR of heartbeat components is low, and heartbeat components tend to be distorted by such noise. Also, even when a subject keeps still, components due to non-heartbeat could remain within the time window even after some signal processing, which could degrade the heartbeat detection accuracy of the conventional methods. In particular, for the subjects with low HR, the estimated HR by the conventional heartbeat detection methods tends to be higher than the ground truth HR. This is because when the SNR of heartbeat components is low, more noise components tend to occur over the received signal. Also, the estimated RRI tends to be shorter than the ground truth RRI, for the subjects with low HR. This is because when the SNR of heartbeat components is low, more noise components tend to appear over the received signal, which makes it challenging to pick up correct peaks due to heartbeat. Here, it is

worth mentioning that the conventional methods have mainly focused on the heartbeat detection against the subjects with the standard HR higher than 50 bpm. Hence, it is necessary to develop a more accurate heartbeat detection method with more robustness to the degradation of the SNR of heartbeat components, and for the low HR subject.

2.2 ECG signal reconstruction

In this section, we describe other existing researches related to ECG signal reconstruction. ECG is a heartbeat detection method that has been widely used in the medical field. Features of an ECG signal, e.g., the P-wave, the T-wave, and the R-peak, reflect the heart activity, and thus it is possible to detect some heart diseases by analyzing an ECG signal. PPG can emit light on the skin and observe the intensity variation of the reflected light. Since such intensity variation reflects the heart's activity, heartbeat can be detected by analyzing a PPG signal. Some researches have proposed accurate heartbeat detection methods with a PPG radar mounted in wrist-type devices such as smart-watches [65]-[67]. Additionally, Q. Zhu *et al.* have proposed an ECG signal reconstruction method via a PPG signal [66]. This method extracts features, i.e., the DCT coefficients of a heartbeat signal, from PPG and ECG signals, and then reconstructs an ECG signal by mapping the DCT coefficients with PPG to those of ECG signals as shown in Fig. 2.3. The experimental results have shown that this method achieves a high correlation coefficient between the estimated and actual ECG signals, i.e., 0.96. In addition to ECG and PPG, SCG has also been used for heartbeat detection [68]-[70]. SCG can detect heartbeat by measuring the chest vibration and capture the aortic valve opening and closing behavior, as well as the mitral valve opening and closing behavior. J. Park *et al.* have proposed a method to transform an SCG signal itself to an ECG signal based on a deep learning model with bidirectional-LSTM [67], as shown in Fig. 2.4. This method has been shown to be able to reconstruct an ECG signal with a high accuracy. Although these ECG signal reconstruction methods have been experimentally shown to be able to reconstruct the ECG signal, PPG and SCG essentially require device attachment.

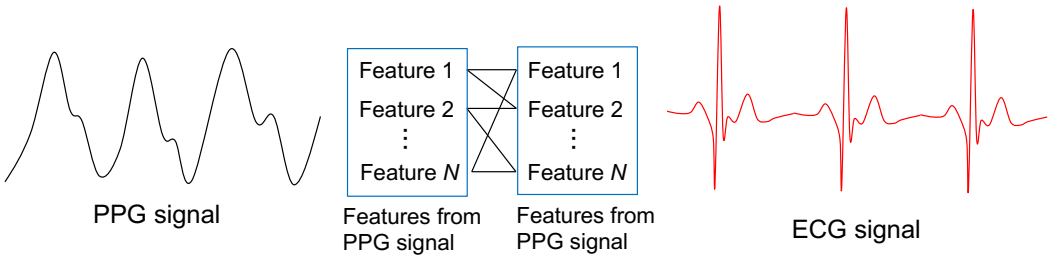

Figure 2.3: The overview of the PPG-based ECG signal reconstruction [66].

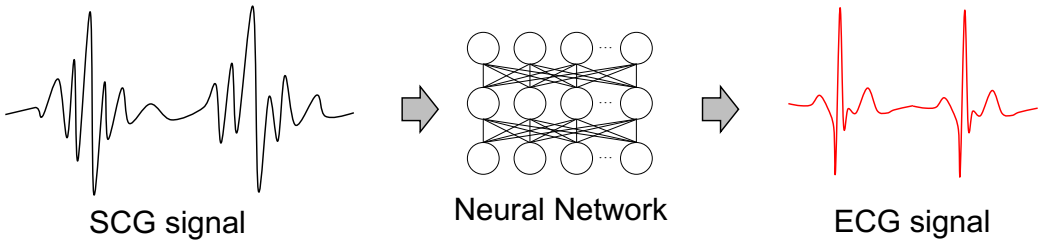

Figure 2.4: The overview of the SCG-based ECG signal reconstruction [67].

2.3 LSTM, CNN, and convolutional LSTM

In this section, for a better understanding of our proposed method, we explain deep learning technique related to our method.

2.3.1 LSTM

In contrast, LSTM is one of Recurrent Neural Network (RNN) that has been broadly used to analyze time sequence data, and it provides excellent performance of the temporal feature extraction [69]. LSTM typically consists of 4 blocks: (i) the LSTM block, (ii) the input gate, (iii) the forget gate, and (iv) the output gate. Now, let y and h denote input data and hidden states, respectively, and let W, R, p, and b denote the weight from the previous layer, the weight from the hidden layer in the previous time, the peephole weight, and the bias, respectively. The forward-propagation of LSTM is operated as follows.

$$z^{-t} = W_z y^t + R_z h^{t-1} + b_z, \tag{2.4}$$

$$z^t = \tanh(z^{-t}), \tag{2.5}$$

$$i^{-t} = W_i y^t + R_i h^{t-1} + p_i \odot c^{t-1} + b_i, \tag{2.6}$$

$$i^t = \mathrm{sigmoid}(i^{-t}), \tag{2.7}$$

$$f^{-t} = W_f y^t + R_f h^{t-1} + p_f \odot c^{t-1} + b_f, \tag{2.8}$$

$$f^t = \mathrm{sigmoid}(f^{-t}), \tag{2.9}$$

$$c^t = i^t \odot z^t + f^t \odot c^{t-1}, \tag{2.10}$$

$$o^{-t} = W_o y^t + R_o h^{t-1} + p_o \odot c^{t-1} + b_o, \tag{2.11}$$

$$o^t = \mathrm{sigmoid}(o^{-t}), \tag{2.12}$$

$$H^t = o^t \odot \tanh(c^t), \tag{2.13}$$

where "$\odot$" is the Hadamard product, and the subscripts "z", "i", "f", and "o" denote the LSTM block, the input gate, the forget gate, and the output gate, respectively.

2.3.2 CNN

CNN is also a deep learning technique that has the great ability of spatial feature extraction [73]. Typically, CNN has two operations: (i) the convolutional operation and (ii) the pooling operation. Here, let $x^l_{i,j}$ and $w_{p,q}$ denote the elements of the feature map in the layer l and the convolutional filter with the kernel size of $P \times Q$, respectively. With the stride size of the convolutional filter s, the convolutional operation is performed as

$$u_{i,j} = \sum_{p=0}^{P-1} \sum_{q=0}^{Q-1} x_{si+p,sj+q} w_{p,q}. \tag{2.14}$$

With the activation function of Rectified Linear Units (ReLU), the enhancement of the extracted feature $u_{i,j}$ is performed, and the element of the feature map in the next layer $x^{l+1}_{i,j}$ is obtained as

$$x^{l+1}_{i,j} = \mathrm{ReLU}(u_{i,j}). \tag{2.15}$$

The pooling operation is performed to reduce the training time by reducing the elements of the feature map, in general. The max pooling algorithm is a typical one used to reduce the size of the feature map and is used in our proposed model. The max pooling algorithm with the pooling area O in the layer l is performed as

$$x^{l+1}_{i,j} = \max_{(p,q) \in O} x^l_{p,q}. \tag{2.16}$$

2.3.3 Convolutional LSTM

Convolutional LSTM is a deep learning technique with both the features of LSTM and the convolutional operation used in CNN [68]. LSTM can extract features of time sequence data [69], and it has been applied for signal classification [55][56] and prediction [57]. Also, CNN has been successfully used in image recognition [59][60], and the convolutional operation is one of the operations in CNN to extract detailed features from image data [73]. With the advantages of LSTM and the convolutional operation, convolutional LSTM has been applied to extract features from the successive image data in the field of object recognition and frame prediction over movie data [62]-[64].

Now, let X and H denote input data and hidden states, respectively. Also, let W, R, p, and b denote the weight from the previous layer, the weight from the hidden layer in the previous time, the peephole weight, and the bias. The forward-propagation of the convolutional LSTM is performed as follows.

$$z^{-t} = W_z * X^t + R_z * H^{t-1} + b_z, \tag{2.17}$$

$$z^t = \tanh(z^{-t}), \tag{2.18}$$

$$i^{-t} = W_i * X^t + R_i * H^{t-1} + p_i \odot c^{t-1} + b_i, \tag{2.19}$$

$$i^t = \mathrm{sigmoid}(i^{-t}), \tag{2.20}$$

$$f^{-t} = W_f * X^t + R_f * H^{t-1} + p_f \odot c^{t-1} + b_f, \tag{2.21}$$

$$f^t = \mathrm{sigmoid}(f^{-t}), \tag{2.22}$$

$$c^t = i^t \odot z^t + f^t \odot c^{t-1}, \tag{2.23}$$

$$o^{-t} = W_o * X^t + R_o * H^{t-1} + p_o \odot c^{t-1} + b_o, \tag{2.24}$$

$$o^t = \text{sigmoid}(o^{-t}), \tag{2.25}$$

$$H^t = o^t \odot \tanh(c^t), \tag{2.26}$$

where the subscripts "z", "i", "f", and "o" denote the LSTM block, the input gate, the forget gate, and the output gate, respectively. Also, "$*$" and "$\odot$" are the convolutional operation and the Hadamard product, respectively.

Chapter 3

Proposed Heartbeat Detection

In this chapter, we describe the proposed heartbeat detection method. In what follows, we first explain the idea of the proposed method in Section 3.1, and then present the algorithm of our proposed method in Section 3.2. We subsequently show the performance of our method through some experiments in Section 3.3. Finally, we conclude this chapter in Section. 3.4

3.1 Idea of proposed method

3.1.1 Heartbeat component extraction

Heartbeat components obtained by a Doppler radar have two kinds of frequency components:

- Frequency components corresponding to the HR
- Frequency components related to just one heartbeat

As we mentioned before, noise components such as respiration and body fluctuation are distributed over the frequency ranges related to the HR. Thus, the heartbeat components tend to be distorted by such noise over the HR ranges. In contrast, frequency components related to just one heartbeat is distributed over higher frequency ranges. Fig. 3.1 shows an example of the spectrogram obtained from a subject holding his breath. In this figure, we can see that the spectrum appears periodically. Each spectrum is caused by one heartbeat. More specifically, the spectrum in the positive frequency domain is associated with heart diastole, while the spectrum in the negative frequency domain is associated with heart systole. Through some preliminary experiments, we

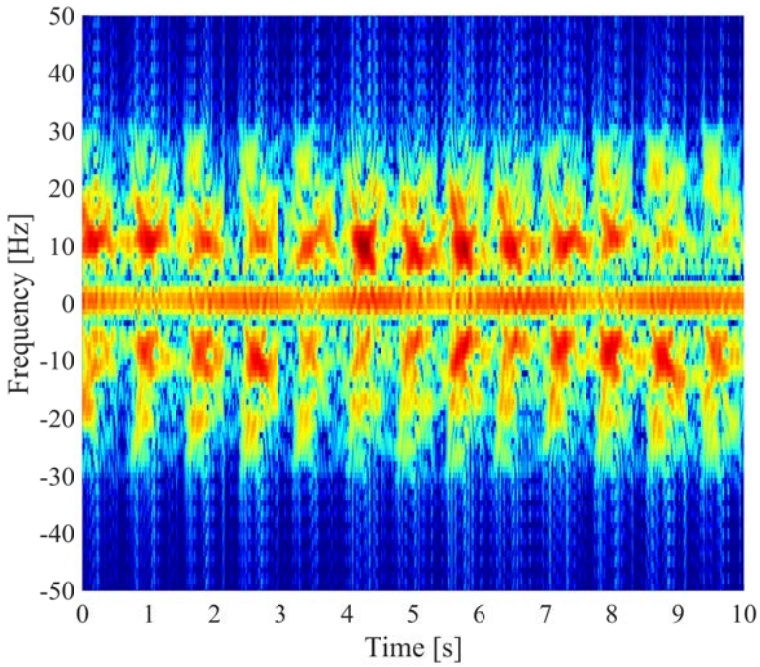

Figure 3.1: An example of a spectrogram obtained from a subject holding his breath.

confirmed that the spectrum due to one heartbeat mainly ranges from 8.0 Hz to 30 Hz and from -30 Hz to -8.0Hz. Here, it is worth mentioning that there could be less effect of such noise over higher frequency ranges related to just one heartbeat, compared to the HR ranges. This is because noise components are distributed over the lower frequency ranges related to the HR as we mentioned above. Fig. 3.2(a) and (b) show examples of the integrated spectrum against a subject sitting still when the detection range is 0.5 m and 2.0 m. Here, note that the integrated spectrum is the time-domain signal obtained by integrating the spectrum for each time over a spectrogram. Also, the corresponding ECG signals are shown, and the amplitudes of these signals are scaled for a better comparison. From Fig. 3.2(a), it can be seen that it could be possible to detect heartbeat by picking up peaks over the integrated spectrum. In contrast, many peaks due to non-heartbeat appear over the integrated spectrum, when the detection range is 2.0 m. This is because as the detection range get long, the SNR of heartbeat components is smaller. Thus, to realize more accurate heartbeat detection based on such high frequency components of heartbeat, we introduce heartbeat signal reconstruction from a spectrogram based on deep learning.

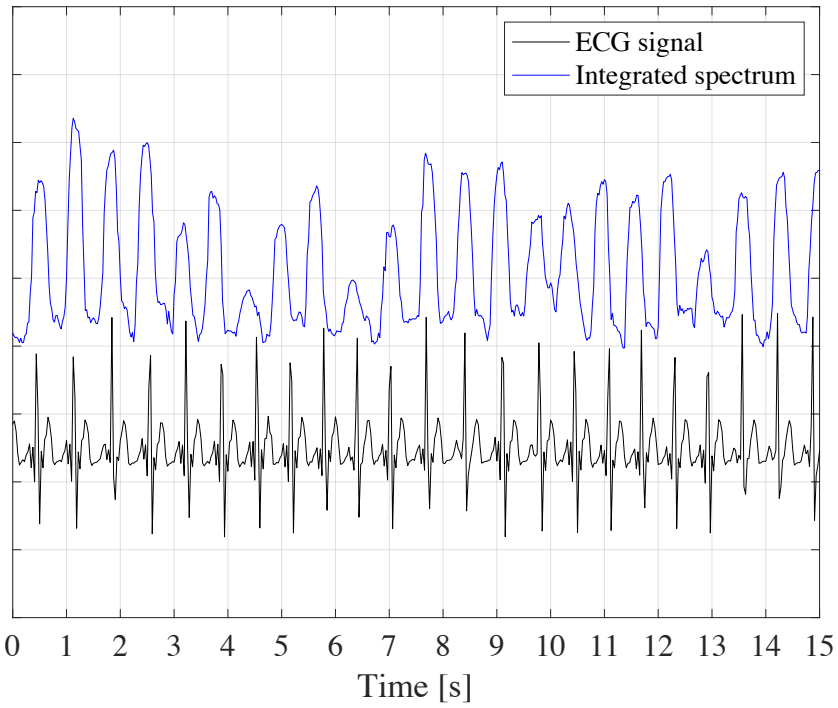

(a) Detection range = 0.5 m

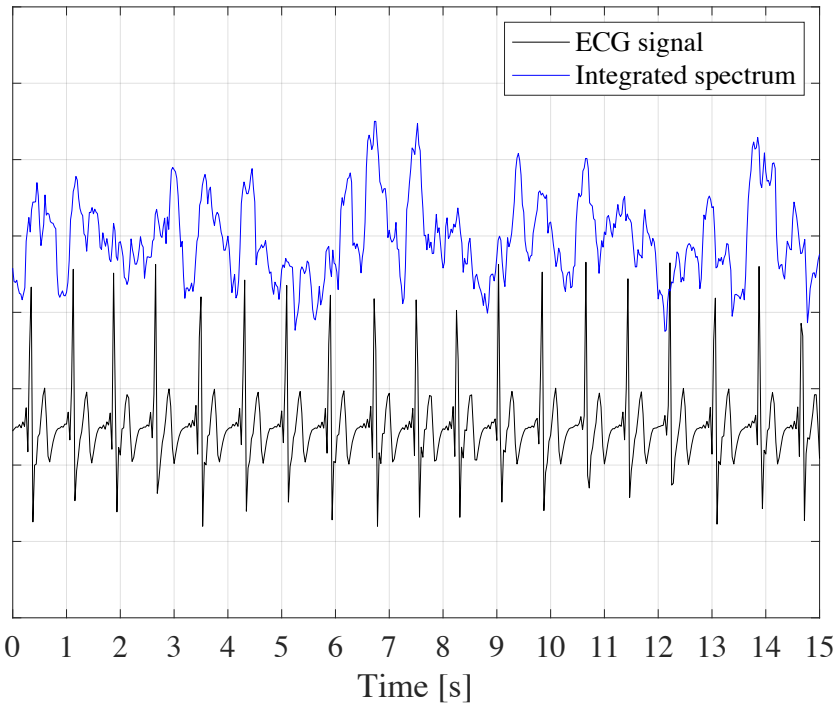

(b) Detection range = 2.0 m

Figure 3.2: Examples of the integrated spectrum against a subject sitting still.

3.1.2 Signal reconstruction based on convolutional LSTM

To reconstruct a heartbeat signal from a spectrogram, we use convolutional LSTM as a deep learning model. As we mentioned in Chapter 2, convolutional LSTM is a deep learning technique that has both the advantages of LSTM and convolutional LSTM, and has been successfully applied for movie data processing such as object recognition. The motivation of using convolutional LSTM is inspired by the characteristic spectrum distribution of heartbeat over a spectrogram. As we can see from Fig. 4.1, heartbeat has two features about spectrum distribution:

- The periodicity of the spectrum, which is caused by several heartbeat
- The spectrum distribution caused by just one heartbeat

Based on this fact, we think that by using successive spectrogram images and convolutional LSTM, it could be possible to consider such two features and to reconstruct a heartbeat signal well.

3.2 Algorithm of proposed method

In this section, we explain the algorithm of the proposed heartbeat detection method based on heartbeat signal reconstruction with convolutional LSTM. Fig. 3.3 shows the flowchart of the proposed heartbeat detection method. Our proposed method consists of two steps, i.e., (i) pre-processing and (ii) heartbeat signal reconstruction with convolutional LSTM, and (iii) peak detection, In what follows, we explain our proposed method in terms of these three steps.

3.2.1 Pre-processing

In the proposed method, after the acquisition of $I(t)$ and $Q(t)$ with the sampling rate of 1000 Hz, a Doppler signal $S(t)$ is firstly calculated as

$$S(t) = I(t) + jQ(t). \tag{3.1}$$

To reduce the effect of non-heartbeat components, e.g., due to respiration and body movements, BPF is applied to the Doppler signal. Based on the fact that the frequency components of heartbeat are distributed mainly within $[8.0, 30]$ Hz [43], the cut-off frequencies of BPF are set as 8.0 Hz and

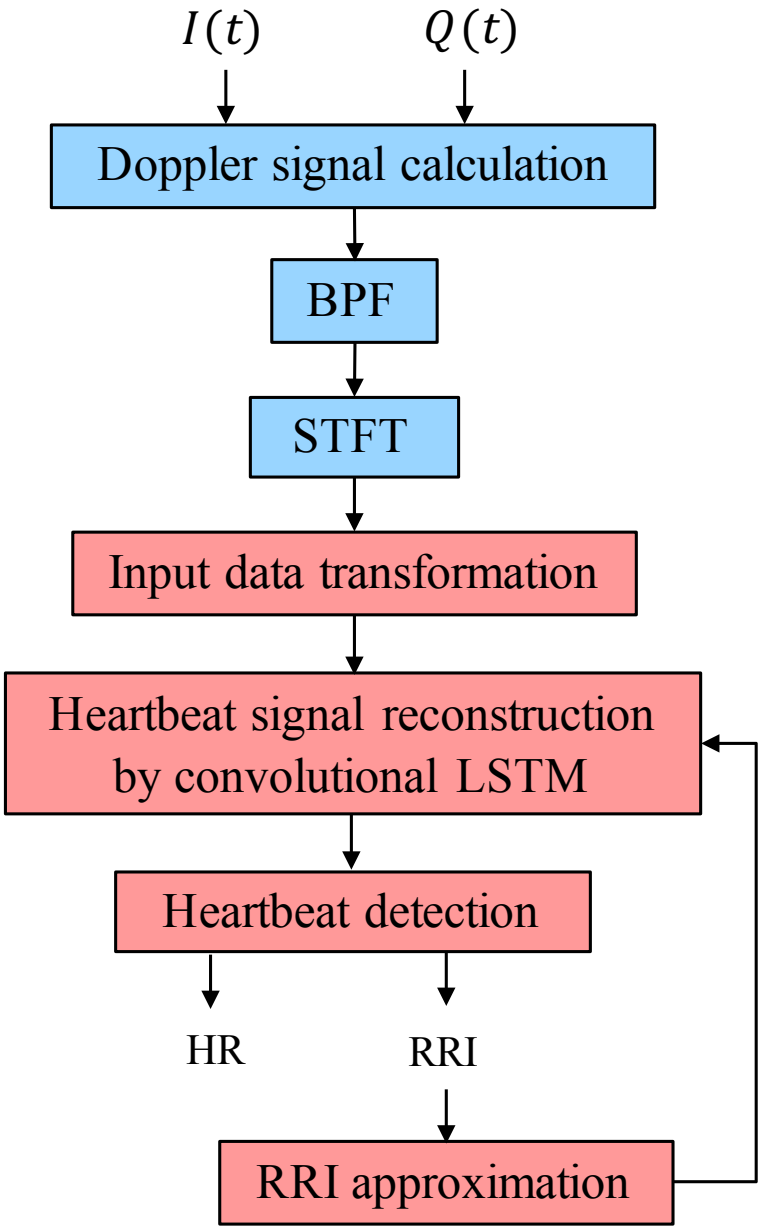

Figure 3.3: The flowchart of the proposed heartbeat detection method.

30 Hz. Short Time Fourier Transform (STFT) is subsequently applied to the filtered signal. The time window size and step size are set as 256 ms and 25 ms, respectively, and these parameters are short enough to analyze the spectrum due to one heartbeat. To accurately extract heartbeat components from a spectrogram, our proposed method reconstructs a heartbeat signal from a spectrogram based on convolutional-LSTM in the next step.

3.2.2 Heartbeat signal reconstruction with convolutional LSTM

Input data transformation

In the proposed method, to realize the fast heartbeat detection, heartbeat is detected with 5 s data, including at least two heartbeats. Fig. 3.4 shows a concept of the input data transformation. The spectrogram is firstly segmented by 5 s-window corresponding to 200 samples. Also, the spectrum in $[8.0, 28]$ Hz and $[-28, -8.0]$ Hz is concatenated as shown in Fig. 3.4(b). The 5 s-segmented spectrogram is then further segmented by 0.25 s time window with the step size with 0.05 s, which results in 95 spectrograms as shown in Fig. 3.4(c). Here, 0.25 s and 0.05 s correspond to 10 samples and 2 samples, respectively, and these parameters are short enough to capture the spectrum distribution peculiar to heartbeat. Eventually, 95 spectrograms sorted with regard to the time order are input to convolutional LSTM, and the size of the input data is $10 \times 10 \times 95$. The input data size is dependent on the step size of the window used in STFT. As the step size gets short, the input data length gets longer, and thus the more features could be extracted by convolutional LSTM. However, the long length of the input data makes it challenging to train the deep learning model, depending on the number of the training data. Based on this fact, the step size of the window is set as 25 ms through the preliminary experiments.

Model architecture

Fig. 3.5 shows the architecture of the proposed deep learning model. The proposed model is based on five layers: (i) the input one, (ii) the convolutional LSTM one, (iii) the concatenate one, (iv) the fully-connected one, and (v) the output one. In the proposed method, two convolutional LSTM layers are used, and the batch normalization is performed after each convolutional LSTM layer to reduce the training time. Here, the kernel size and the number of filters in convolutional LSTM

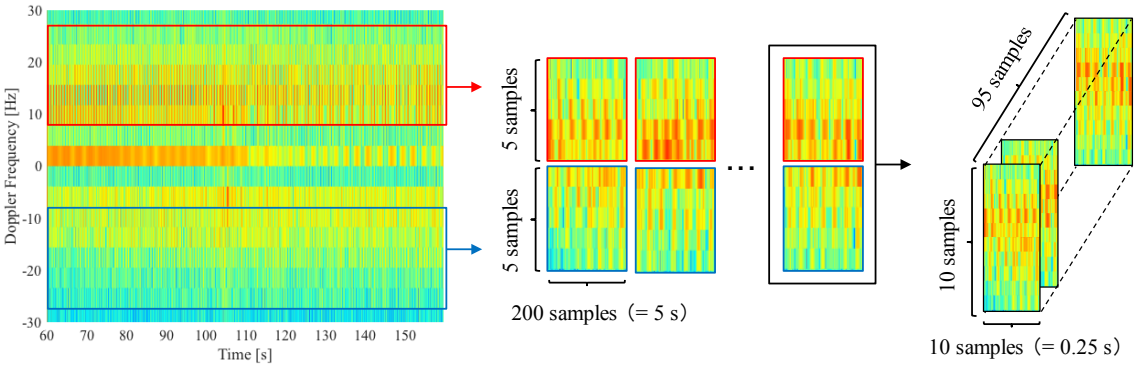

(a) Spectrogram (b) Segmentation (c) Input data

Figure 3.4: A concept of the input data transformation.

are 3×3 and 32, respectively. These parameters should be set considering the over-learning and the reconstruction accuracy of a heartbeat signal, and these can be adjusted depending on the diversity and the number of training data. After the convolutional LSTM layers, to better reconstruct a heartbeat signal, RRI_{prev} is calculated as the average value of the RRIs estimated from the previous output, and then RRI_{prev} is inputted to the model by concatenating it with the output of the convolutional LSTM layers. However, there exist numerous candidates of RRI_{prev}, which makes it difficult to train the deep learning model as well as the long length of the input data. Based on this fact, in the proposed method, a set of 32 RRI candidates, i.e., 500 ms, 550 ms, 600 ms, ..., 2000 ms is defined considering the number of training data. RRI_{prev} is approximated to the RRI that is closest to RRI_{prev} among 32 RRI candidates. In the initial observation where RRI_{prev} is not available, the model without RRI_{prev} is used. The fully-connected layer consists of two layers with 1,024 units. As an output of our model, the ECG signal, which is filtered by BPF with its cut-off frequencies 0.5 Hz and 2 Hz, is used. The sampling rate of the ECG signal is initially 200 Hz, and the sampling rate is downsampled to 40 Hz. Thus, the output data length is 200, corresponding to 5 s. Also, to reconstruct a heartbeat signal considering the periodicity of heartbeat, as the loss function L, the correlation coefficient between the predicted output and the

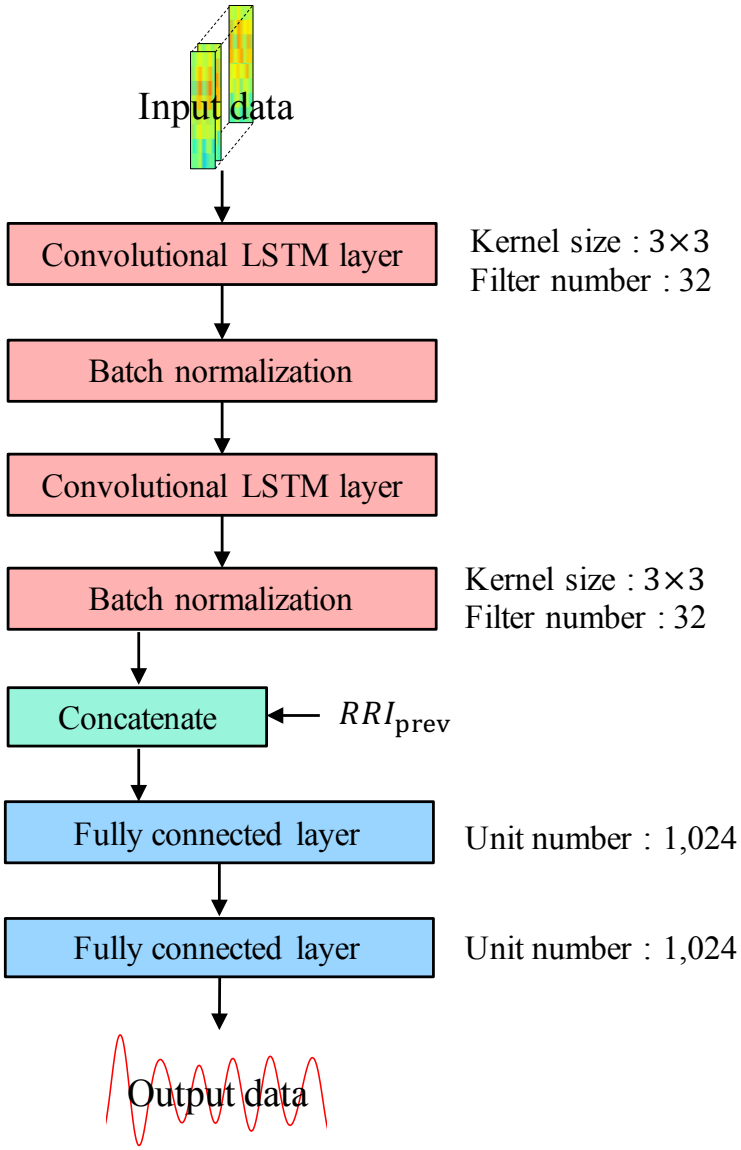

Figure 3.5: The architecture of the proposed deep learning model.

true output, c, is used as

$$L = 1 - c. \tag{3.2}$$

3.2.3 Peak detection

After acquiring the output signal of the model, heartbeat could be detected by selecting peaks of the output signal. However, undesired peaks sometimes appear over the output signal. To detect heartbeat incorrectly, in the proposed method, BPF is applied to the output signal, where its cut-off

frequencies are set as 0.5 Hz and 2.0 Hz, corresponding to 30 bpm and 120 bpm. Peaks are then detected as heartbeat over the filtered output signal.

3.3 Performance evaluation

3.3.1 Perfomance metrics

To evaluate the heartbeat detection accuracy of the proposed method, we conducted the experiments to observe heartbeat from subjects with not only normal HR but also low HR. As the performance metric, we calculated the Root Mean Squared Error (RMSE) between the estimated and ground-truth RRIs.

$$RMSE = \sqrt{\frac{1}{N}\sum_{i=1}^{N} |RRI_{\mathrm{est}}(i) - RRI_{\mathrm{ref}}(i)|^2}, \tag{3.3}$$

where N denotes the number of the observed RRIs. i also denotes the time when the i th peak appears, and RRI_{est} and RRI_{ref} denote the estimated RRI and the ground truth value of the RRI, respectively. In addition to the RMSE, we also calculated the Average Absolute Error (AAE) between the estimated and ground truth HRs, and the Average Relative Error (ARE) of the HR.

$$\mathrm{AAE} = \frac{1}{M}\sum_{j=1}^{M} |HR_{\mathrm{est}}(j) - HR_{\mathrm{ref}}(j)|, \tag{3.4}$$

$$\mathrm{ARE} = \frac{1}{M}\sum_{j=1}^{M} \frac{|HR_{\mathrm{est}}(j) - HR_{\mathrm{ref}}(j)|}{HR_{\mathrm{ref}}(i)}, \tag{3.5}$$

where M denotes the number of the observed HRs, $HR_{\mathrm{est}}(j)$ and $HR_{\mathrm{ref}}(j)$ denote the j th estimated and ground truth HRs, respectively. Here, note that the HR is estimated by calculating the reciprocal of the average value of the estimated RRIs within 5 s, which is performed by 5 s-time window with the step size of 2 s.

3.3.2 Experimental setup

TABLE 3.1 lists the experimental specification. In the experiments, we used a 24 GHz Doppler radar with a sampling rate of 1000 Hz. To collect the training data, we observed heartbeat against eight subjects sitting still for 240 s. Also, to extend the diversity of the HR variation over the training data, we interpolated the input and output data as the following steps: (i) R-peaks were detected over the ECG signal, (ii) the timing when heartbeat did not occur was detected based on the results of the first step, and (iii) the input and output data were interpolated by the AR (Autoregressive) model. We collected 10,350 training data with the HR of $[30, 120]$ bpm through this extension of the training data. In contrast, as the testing data, we observed heartbeat against 17 subjects with the Doppler radar attached to the ceiling. Here, it is worth mentioning that the subjects for the testing data were different from the ones for the training data. TABLE 3.2 lists the testing dataset. The subjects 1, 2, 3, 4, and 5 were sitting still at 1.0 m away from the Doppler radar, and the subjects 6, 7, 8, 9, and 10 were lying up on the floor at 2.5 m away from the Doppler radar. Also, the subjects 11, 12, 13, 14, 15, 16, and 17 were lying up on the bed, and the distance between a subject and the Doppler radar attached on the ceiling was about 2.0 m. The observation time is 180 s for each subject. To collect the output data of the proposed deep learning model and to measure the ground true RRI and HR, we used ECG with the sampling rate of 200 Hz. The optimizer to train the model was "RMSprop", the number of epochs was 50, and the batch size was 256.

3.3.3 Results

Performance of heartbeat signal reconstruction

Fig. 3.6 shows the training and the validation losses, where the validation rate is 10 %. As can be seen from this figure, the training loss converges at about 0.15, i.e., the correlation coefficient c is 0.85, and the validation one does at about 0.25, i.e., c is 0.75. Fig. 3.7 shows examples of ECG signal, the integrated spectrum, and the output signal of the proposed deep learning model with convolutional LSTM. In Figs. 3.7(a) and (b), for the better comparison, the amplitudes of these three signals are scaled. From these figures, it can be seen that many peaks due to non-heartbeat appear over the integrated spectrum, which could degrade the heartbeat detection accuracy. In

Table 3.1: Testing dataset.

Item	Value
Modulation method	Unmodulated continuous wave
Carrier frequency	24 GHz
Sampling rate of Doppler radar	1000 Hz
The number of subjects	17
Observation duration	180
Detection range d	From 1.0 m to 2.5 m
Sampling rate of ECG	200 Hz
Optimizer to train mode	RMSprop
Epochs to train model	50
Batch size to train model	256

particular, the HR estimated based on the integrated spectrum tends to be higher than the ground truth HR because of such incorrect peak. In contrast, from these figures, it can be seen that less peaks due to non-heartbeat appear over the output signal of the proposed model, which could bring the improvement of the heartbeat detection accuracy.

Performance of the proposed method

Figs. 3.8 and 3.9 show examples of the RRI and HR estimation results. In these figures, our previous heartbeat detection method [43] estimates the HR by calculating the reciprocal of the average value of the detected peak-to-peak intervals within 5 s as well as the proposed one. As can be seen from these figures, some estimated RRIs and HRs by our previous method are inaccurate due to the incorrect peak detection, particularly for the subject with low HR. In contrast, the proposed method, including the one without the input of RRI_{prev} improves the heartbeat detection accuracy of our previous one, in particular for the subject with low HR. Furthermore, thanks to the

Table 3.2: Testing dataset.

ID	Sex	Ave. RRI [ms]	Ave. HR [bpm]	d [m]
1	M	782	76.7	1.0 m
2	M	801	74.9	1.0 m
3	F	681	88.1	1.0 m
4	M	924	64.9	1.0 m
5	M	874	68.6	1.0 m
6	M	886	67.8	2.5 m
7	M	659	90.9	2.5 m
8	F	887	67.6	2.5 m
9	F	818	73.4	2.5 m
10	F	837	71.6	2.5 m
11	M	1,293	46.5	2.0 m
12	M	1,111	54.1	2.0 m
13	M	1,486	40.4	2.0 m
14	M	1,040	57.8	2.0 m
15	M	1,508	39.8	2.0 m
16	M	1,308	45.8	2.0 m
17	F	1,292	46.4	2.0 m

heartbeat signal reconstruction with the additional input to the model, i.e., RRI_{prev}, the proposed method reconstructs a heartbeat signal better. Thus, it provides the most accurate RRI and HR than the other ones do. TABLE 3.3 lists the RMSEs and AAEs of our previous [43] and proposed methods. From this table, it can be seen that the proposed method outperforms our previous ones by the average RMSE and AAE. In particular for the subjects with the HR lower than 50 bpm, i.e., the subjects 11, 13, 15, 16, and 17, our proposed method improves the RMSE and the AAE of our previous one significantly, though the RMSEs and AAEs are higher than those of the other subjects, since the HR variations of the subjects with low HR are large. As a result, our previous

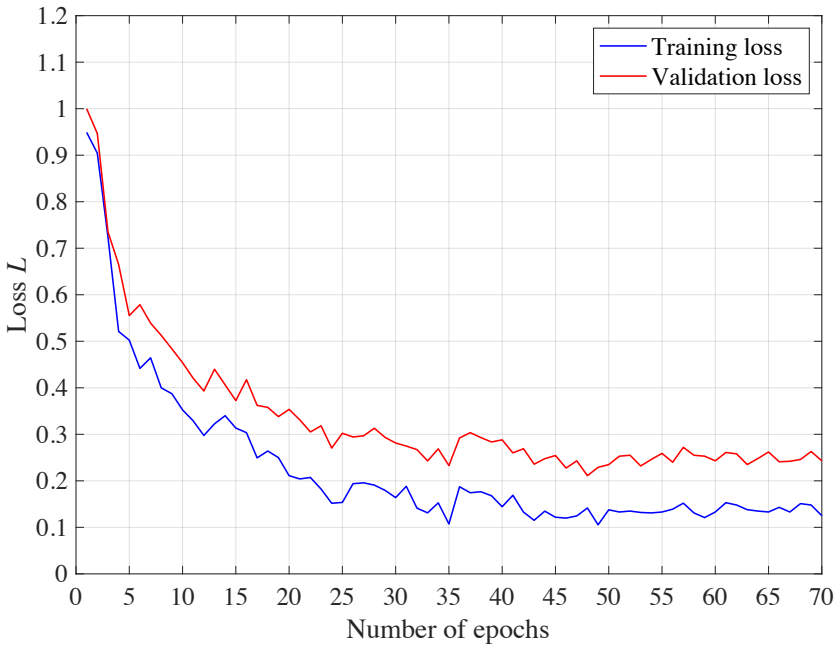

Figure 3.6: The training and validation losses. The validation rate is 10 %.

method's average RMSE and AAE is 308 ms and 13.8 bpm, respectively, while those of our proposal are 111 and 3.84 bpm, respectively. Considering that the HR could be lower and lower at abnormal events such as the onset of the disease, it is worth noting that the proposed method detects heartbeat even with low HR.

Performance comparison of the proposed and existing methods

TABLE 3.4 lists the AAEs and the AREs of the other existing fast heartbeat detection methods that have a short time window and have been evaluated at the long detection range, e.g., at least 1.0 m. In terms of the ARE, the conventional method [13] achieves the ARE of 3.38 % in the situation where the detection range d ranges from 1.0 m to 1.5 m and the HR range to detect heartbeat, R, ranges from 50 bpm to 100 bpm. In contrast, the ARE of our proposed method is 5.04 % in the situation where d ranges from 1.0 m to 2.5 m and R ranges from 30 bpm to 120 bpm. More specifically, the ARE of our proposal is 4.01 % in the situation where R ranges from 50 bpm to 120 bpm, while the ARE is 6.84 % in the situation where R is lower than 50 bpm. Also, in terms of the AAE, our method achieves the small AAE of 3.84 bpm, which is almost equal to

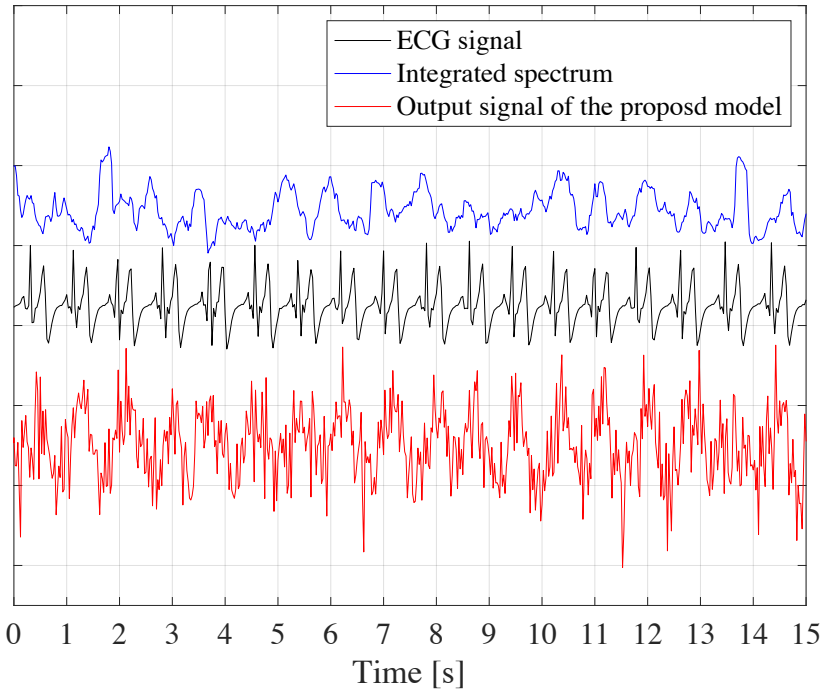

(a) The subject with the normal HR.

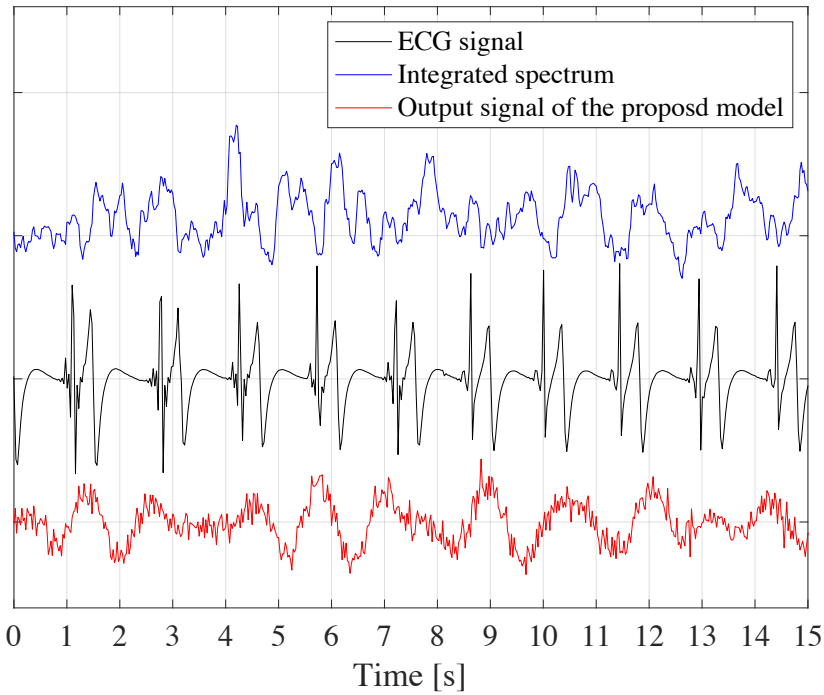

(b) The subject with low HR.

Figure 3.7: Examples of the ECG signal, the integrated spectrum, and the output signal of the proposed deep learning model.

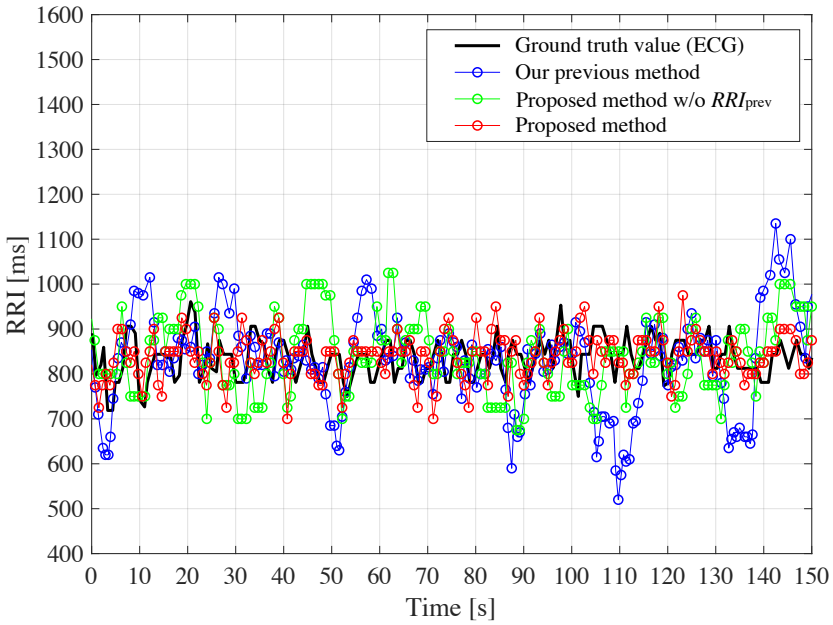

(a) The RRI estimation result.

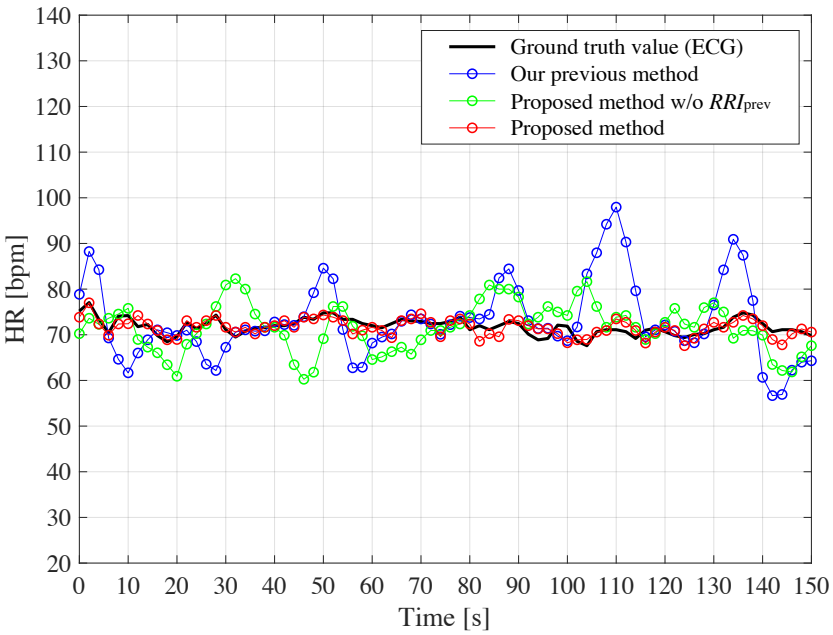

(b) The HR estimation result.

Figure 3.8: The RRI and HR estimation results against the subject 10 with the average HR of 71.6 bpm. The proposed method w/o RRI_{prev} denotes the one that does not use RRI_{prev} as an input to the model.

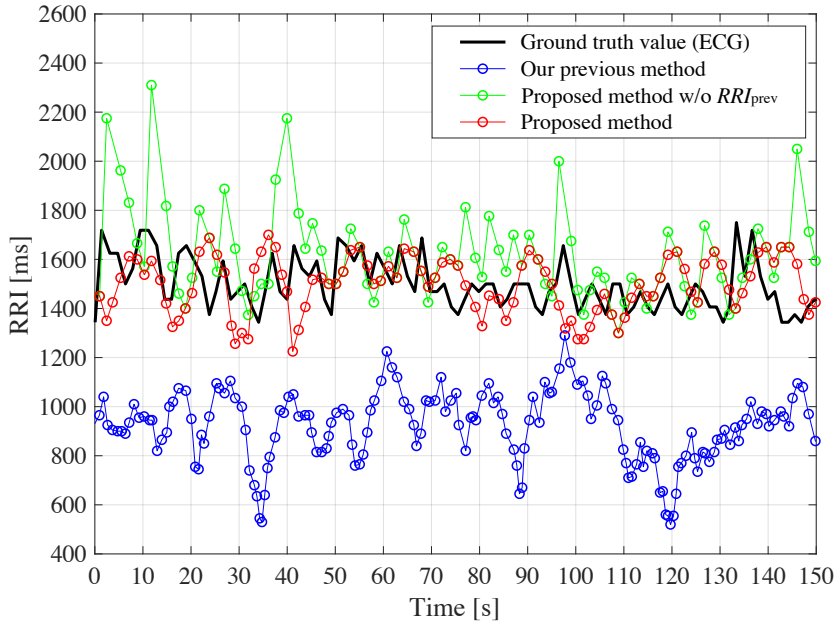

(a) The RRI estimation result.

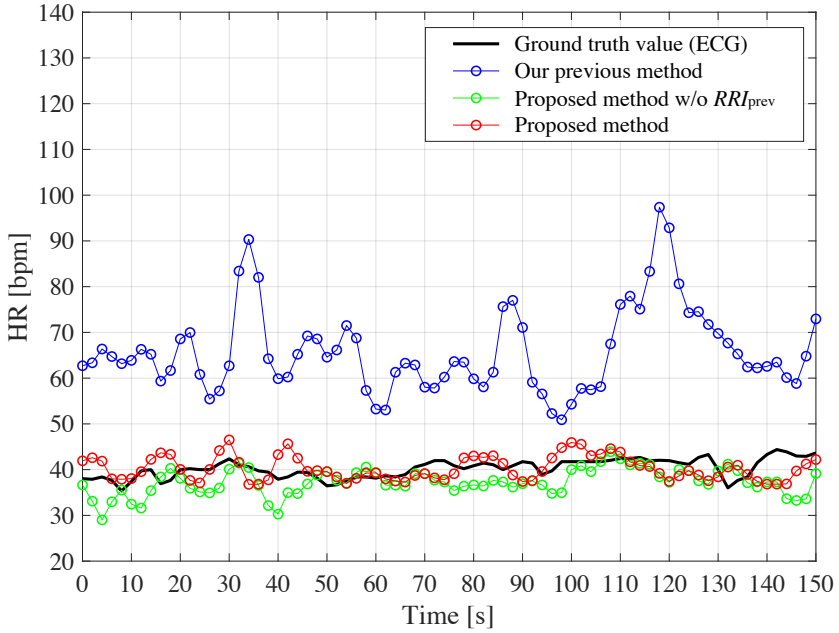

(b) The HR estimation result.

Figure 3.9: The RRI and HR estimation results against the subject 13 with the average HR of 40.4 bpm. The proposed method w/o RRI_{prev} denotes the one that does not use RRI_{prev} as an input to the model.

4.32 bpm and 3.75 bpm of the conventional ones [23] and [24], respectively. Here, note that the conventional one [23] has been evaluated in the situation where d is 1.0 m and R ranges from 60 bpm to 120 bpm, and the one [24] has been done in the situation where d ranges 1.0 m to 1.1 m and R ranges from 51 bpm to 120 bpm. Although the ARE by our proposed method is lower than that of the conventional one [13], these results show that even though the detection range gets long, e.g., 2.0 m, our method performs accurate heartbeat detection even against the subjects with low HR.

3.4 Conclusion

In this chapter, to accurately detect heartbeat via a Doppler radar, we proposed a heartbeat detection method based on heartbeat signal reconstruction with convolutional LSTM. Specifically, we construct a deep learning model with convolutional LSTM to reconstruct a heartbeat signal. To reconstruct a heartbeat signal based on the periodicity of heartbeat and the spectrum distribution peculiar to heartbeat, successive spectrograms within the frequency range that might be related to heartbeat is input to convolutional LSTM, The experimental results showed that even in the situation where the detection range is extended, e.g., 2.0 m, and the SNR of heartbeat components is low, our proposed method achieved the small AAE of 3.84 bpm against 17 subjects including 5 subjects with the HR lower than 50 bpm.

Table 3.3: RMSEs and AAEs of our previous and the proposed methods.

ID	d [m]	Actual Ave. HR [bpm]	RMSE [ms]			AAE [bpm]		
			[43]	Propsal w/o RRI_{prev}	Propsal	[43]	Propsal w/o RRI_{prev}	Propsal
1	1.0	76.7	92	72	73	3.49	3.75	3.56
2	1.0	74.9	109	81	75	5.35	4.48	4.32
3	1.0	88.1	84	62	51	4.29	4.01	3.54
4	1.0	64.9	113	88	81	4.82	4.28	3.91
5	1.0	68.6	81	59	60	3.89	3.77	3.50
6	2.5	67.8	162	122	104	5.13	3.05	3.15
7	2.5	90.9	201	153	129	9.02	4.81	3.02
8	2.5	67.6	145	114	97	6.26	4.48	3.95
9	2.5	73.4	182	119	107	8.22	4.55	4.08
10	2.5	71.6	167	132	109	7.34	4.04	2.79
11	2.0	46.5	623	238	156	27.5	6.08	5.13
12	2.0	54.1	592	185	134	25.2	5.72	4.29
13	2.0	40.4	572	202	139	28.1	3.46	2.77
14	2.0	57.8	368	209	123	10.3	4.23	4.34
15	2.0	39.8	732	237	182	34.7	6.71	5.33
16	2.0	45.8	539	142	122	28.5	3.95	3.84
17	2.0	46.4	481	163	149	22.3	5.10	4.79
Ave.	-	-	308	140	**111**	13.8	4.49	**3.84**

Table 3.4: Performance comparison of the proposed and the conventional fast heartbeat detection methods.

Method	f_c [GHz]	N_s	T_e [s]	d [m]	R [bpm]	T_w [s]	AAE [bpm]	ARE [%]
[13]	5.8 GHz	4	30	1.0 - 1.5	50 - 100	2 - 5	-	3.38
[23]	24 GHz	5	180	1.0	60 - 120	2 - 5	4.32	-
[24]	10.225 GHz	15	80 - 90	1.0 - 1.1	51 - 120	3	3.75	-
Proposal	24 GHz	12	180	1.0 - 2.5	50 - 120	5	3.62	4.01
		5		2.0	Lower than 50		4.37	6.84
		17		1.0 - 2.5	30 - 120		3.84	5.04

f_c : Radar frequency, N_s : Number of subjects, T_e : Observation duration
d : Detection range, R : HR range to detect heartbeat, T_w : Window size to detect heartbeat

Chapter 4

Proposed ECG Signal Reconstruction

In this chapter, we describe the proposed ECG signal reconstruction. We first explain the idea of the proposed method in Section 4.1. We then explain the algorithm of our proposed method in Section 4.2, and evaluate performance of our method in Section 4.3. We finally conclude this chapter in Section 4.4.

4.1 Idea of proposed method

As we mentioned before, frequency components due to heartbeat can be divided into

- Components corresponding to the HR
- Components corresponding to just one heartbeat

In terms of the HR, the frequency components of heartbeat typically range from 0.5 Hz to 2.0 Hz, corresponding to 30 bpm and 120 bpm, respectively. In contrast, the chest's displacement due to heartbeat, x_h, can be expressed as [86].

$$x_h(t) = \nu \cos\{\omega t + \gamma \sin(\Omega t)\}\, e^{-\frac{(t-b)^2}{c}}, \tag{4.1}$$

where ω and Ω are the parameters used to determine the peak location of a heartbeat signal, and ν and γ are the parameters used to determine the magnitude of the peak. Additionally, b and c are the constant parameters. Based on this model, the previous research [42] has generated the simulated

heartbeat signal obtained by a Doppler radar and has shown that the frequency components due to the heartbeat signal are distributed in the higher frequency band.

Fig. 4.1 shows an example of a spectrogram obtained from a subject holding his breath again. This spectrogram is calculated by STFT with a 256 ms-time window and a 5 ms-step size. Also, the sampling rate of the Doppler radar is 1000 Hz, and the number of points in FFT is 1024. From this figure, it can be seen that the spectrum due to each heartbeat appears in the frequency band higher than 2 Hz. As aforementioned, the frequency components due to one heartbeat are mainly distributed from 8.0 Hz to 30 Hz. To associate features of the heartbeat signal with those of the ECG signal, the heartbeat components in such a high-frequency band are essential. Fig. 4.2 shows examples of raw in-phase and quadrature signals and the ones filtered by Band Pass Filter with a passband of $[8.0, 30]$ Hz. For a better comparison, an ECG signal is also shown in Fig. 4.2(c), and the amplitudes of the signals are scaled in Figs. 4.2(b) and (c). From these figures, we can see the heartbeat signal corresponding to the ECG signal over the filtered in-phase and quadrature signals. However, we can also see that the heartbeat signal waveforms are not always the same. Hence, to reconstruct an ECG signal from such heartbeat signal waveforms obtained by a Doppler radar, it is necessary to consider the distortion of the heartbeat waveforms.

To deal with this, we use CNN and LSTM for ECG signal reconstruction. As we explain in Chapter 2, CNN and LSTM have a great ability of extraction spatial and temporal features, respectively. The spatial feature extracted by CNN could lead to the robustness to the waveform distortion. Also, the temporal features are very essential to relate a Doppler radar signal to an ECG signal, and the deep temporal features could be extracted by LSTM. Based on these viewpoints, we use the CNN and LSTM for ECG signal reconstruction with robustness to diversity of heartbeat signal waveforms.

4.2 Algorithm of proposed method

In this section, we describe the algorithm of our proposed method in terms of (i) input data segmentation and (ii) ECG signal reconstruction with CNN and LSTM. Fig. 4.3 shows the flowchart of the proposed ECG signal reconstruction. As can be seen from this flowchart, the proposed method performs ECG signal reconstruction based on the result of heartbeat detection.

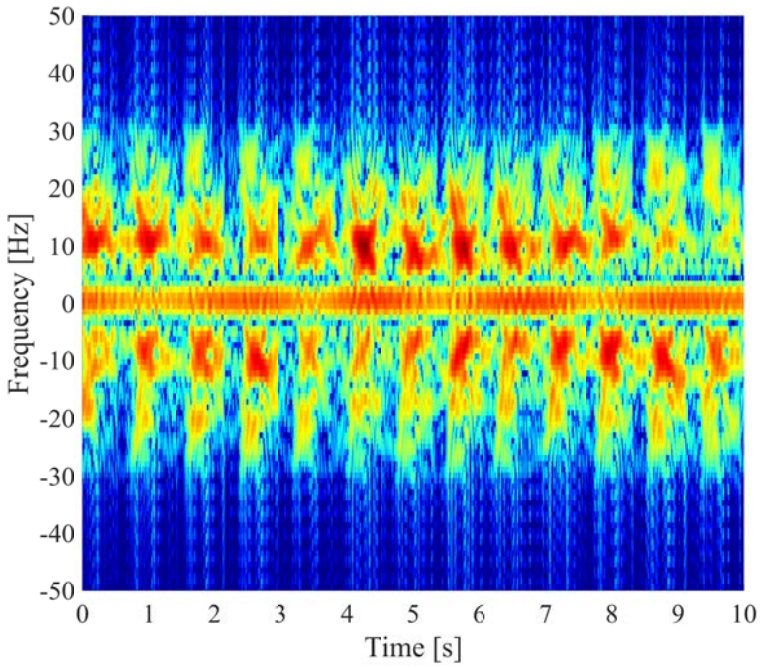

Figure 4.1: An example of a spectrogram obtained from a subject holding his breath.

Input data segmentation

In the proposed method, after detecting heartbeat timing by a heartbeat detection method via the Doppler radar with a sampling rate of 1000 Hz, a heartbeat signal is segmented by a 1.2 s-time window centered at the detected timing as shown in Fig. 4.4. Here, the time window length should be set to include at least one heartbeat, which is very important for reconstructing an ECG signal. In fact, as the heart rate gets low, the timing when the T-wave appears is likely to be delayed. Based on this fact, we selected a 1.2 s-time window that is long enough to meet this condition. Although a subject who has an ECG signal longer than 1.2 s may exist, it is possible to change the window length used in our method. More specifically, as aforementioned, the $I(t)$ and the $Q(t)$ filtered by BPF with the passband of $[8.0, 30]$ Hz are segmented as the heartbeat signal. The segmented $I(t)$ and $Q(t)$ are then input into a deep learning model.

ECG signal reconstruction with CNN and LSTM

In the proposed method, an ECG signal is reconstructed by a hybrid model with CNN and LSTM. Fig. 4.5 shows the architecture of the proposed deep learning model. In the proposed method, the segmented $I(t)$ and $Q(t)$ is concatenated, which is input with the size of 2×800. First, the input is fed into CNN to extract spatial features over the heartbeat signal. This operation makes the model

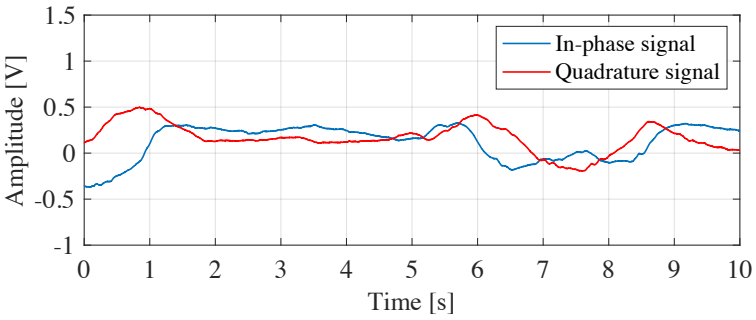

(a) Raw in-phase and quadrature signals

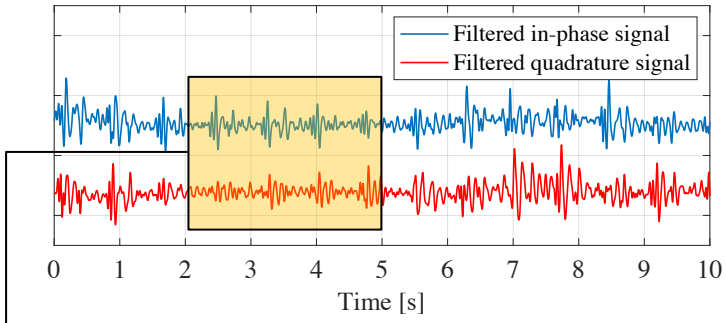

(b) Filtered in-phase and quadrature signals

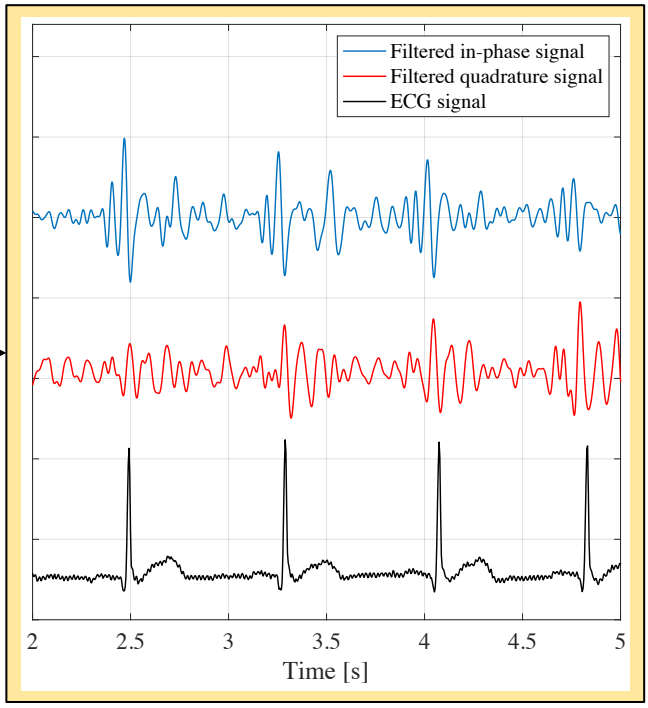

(c) Zoomed filtered in-phase and quadrature signals

Figure 4.2: Examples of raw in-phase and quadrature signals, and the ones filtered by BPF with the passband of $[8.0, 30]$ Hz.

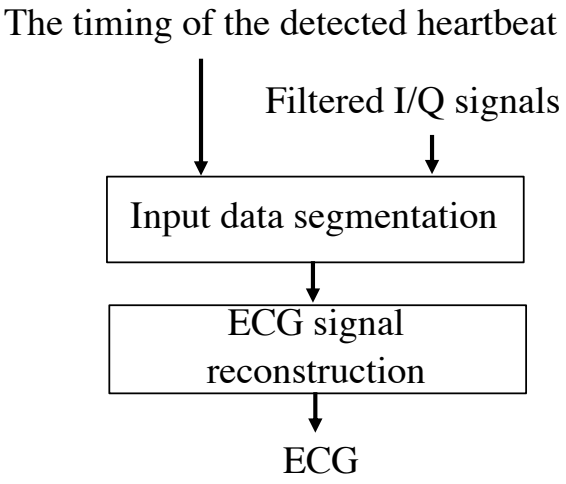

Figure 4.3: The flowchart of the proposed ECG signal reconstruction.

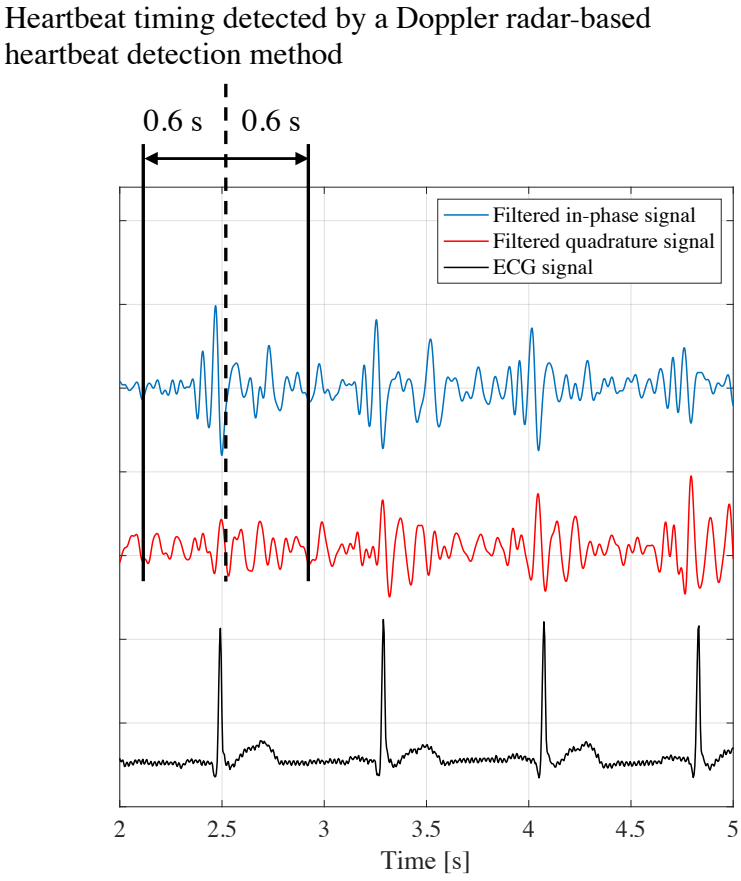

Figure 4.4: Segmentation of input data to a deep learning model.

robust against the deformation of the heartbeat signal. Specifically, the convolutional operation by 8 filters with the kernel size of 2×50 is performed, and then the max pooling operation with the kernel size of 1×2 is performed, where the convolutional filter strides by 1 sample, and the pooling area strides without the overlap. Subsequently, the convolutional operation by 8 filters with the kernel size of 2×25 is performed, and then the max pooling operation with the kernel size of 2×2 is performed. Here, the strides of the convolutional filter and the pooling area are the same as mentioned above. To relate the temporal features of the heartbeat signal to those of the ECG signal, the extracted feature maps are then input to LSTM with 256 hidden layers. Specifically, the output of the CNN can be regarded as the sequence data with a size of 176×8 (data length $\times$ dimension of features), which is an input to LSTM. Through the fully connected layers with 1024 units, the ECG signal is finally output based on the features obtained by the CNN and LSTM. Here, it is worth mentioning that these parameters used in the model, e.g., the number of filters and the kernel size, should be set considering the over-learning and the reconstruction accuracy of the ECG signal. These can also be adjusted depending on the diversity and the number of training data. As for the number of epochs, we set it based on the convergence of the validation loss. Fig. 4.6 shows the training and validation losses. From this figure, it can be seen that the validation loss converges at about 0.015 after epoch 30. In contrast, the training loss decreases slowly even after epoch 30. In fact, when the training loss continues to decrease in such a way, which brings the over-learning. Based on this fact, we set the epoch as 40.

4.3 Performance evaluation

In this section, we first explain the specification of the experiments and then present the experimental results.

4.3.1 Experimental setup

To evaluate the ECG signal reconstruction accuracy of the proposed method, we carried out experiments to collect testing and training data. TABLE 4.1 lists the experimental specification. We carried out our experiments using a 24 GHz Doppler radar with a sampling rate of 1000 Hz, which is the same as the one mentioned in the previous chapter. We observed heartbeat of 9 subjects for

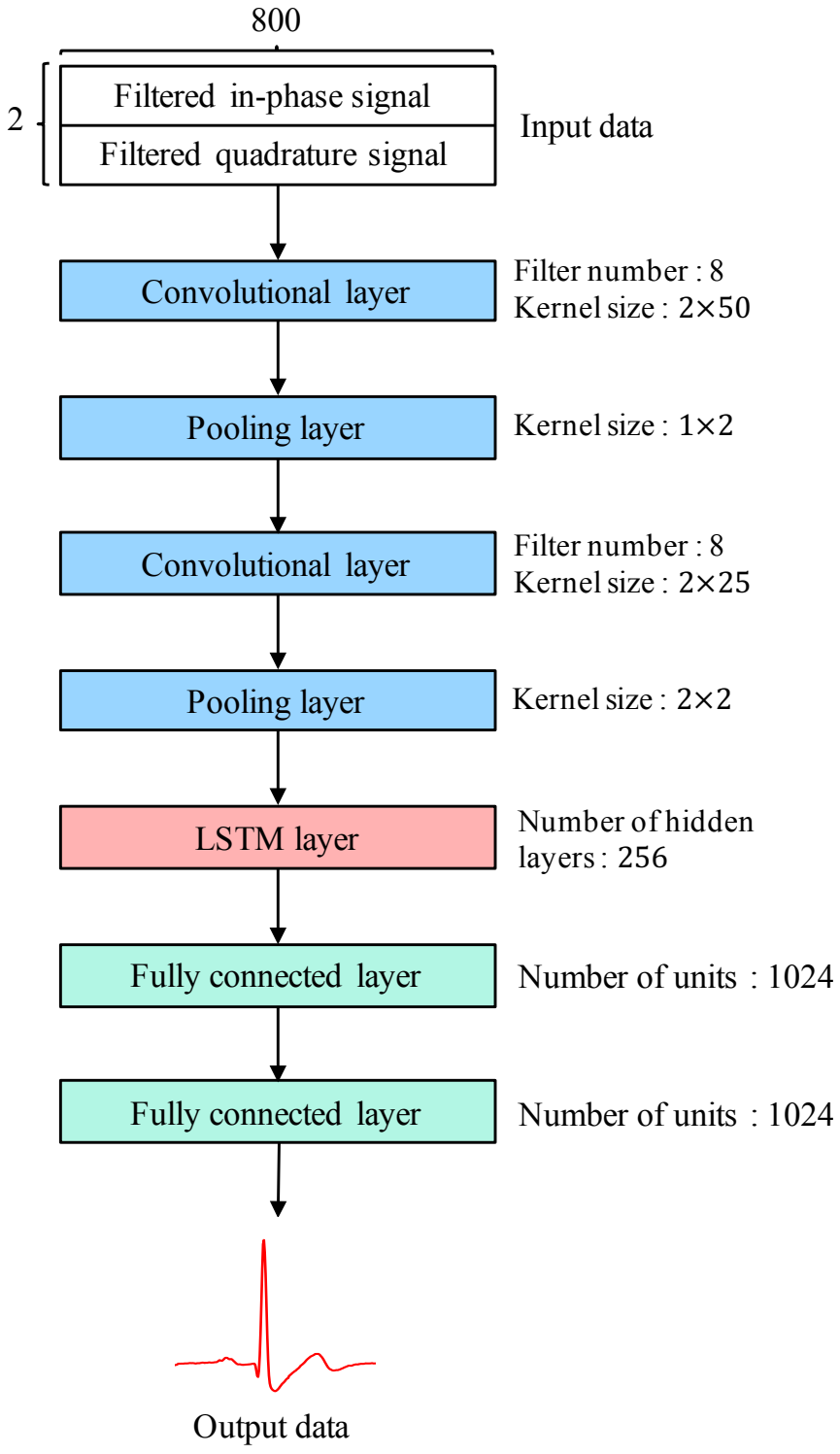

Figure 4.5: The architecture of the proposed deep learning model..

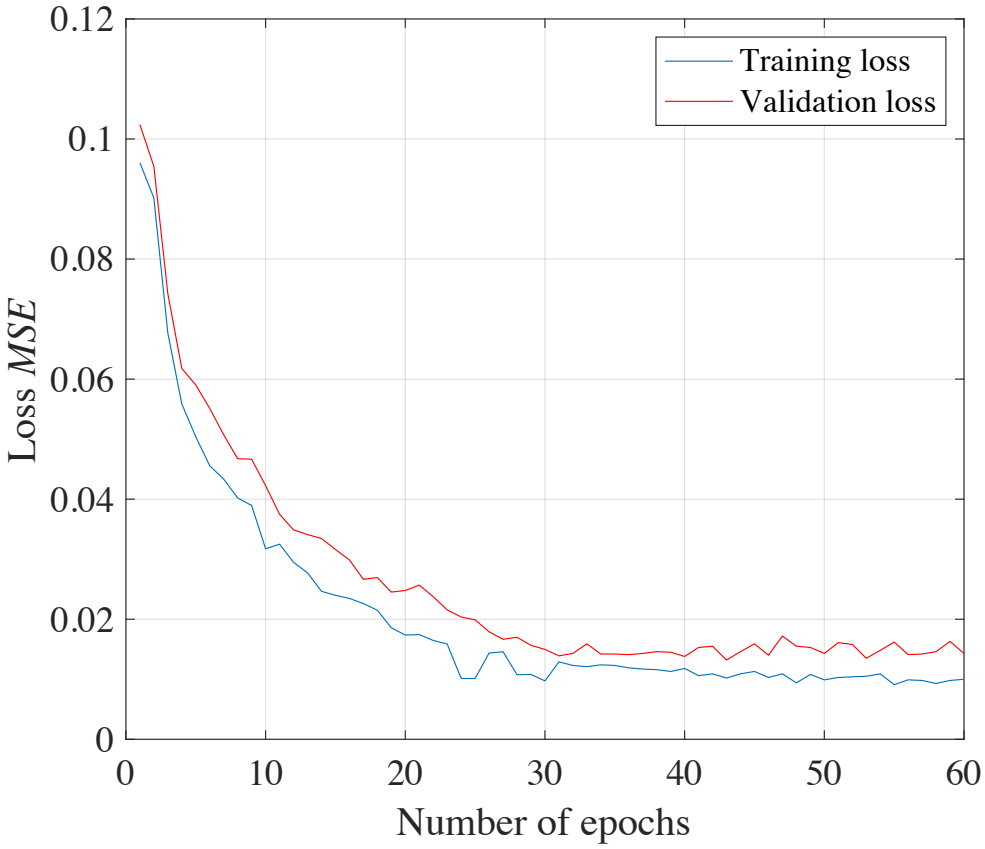

Figure 4.6: The training and validation losses.

Table 4.1: The specification of the experiment.

Item	Value
Modulation method	Unmodulated continuous wave
Carrier frequency	24 GHz
Sampling frequency	1000 Hz
The number of subjects	9
Observation duration	180 s
Detection range	2.5 m
Optimizer to train model	Adam
The number of epochs to train model	40
Batch size to train model	128

180 s, and all the subjects were healthy and did not have abnormalities related to the heart. During the observation, the subjects were lying up on the floor with natural breathing. The Doppler radar was attached to the ceiling, and the distance between the Doppler radar and the subject was 2.5 m. At the same time as the Doppler radar is used to collect the actual ECG signal, we observed the subject's heartbeat by an ECG with a sampling rate of 250 Hz. Also, as the loss function to train the proposed model, we used the Mean Squared Error (MSE). The optimizer used to train the model was "Adam", and the number of epochs and the batch size were 40 and 128, respectively.

4.3.2 Perfomance metrics

As the performance metric, we calculated the correlation coefficient κ between the reconstructed and actual ECG signals as

$$\kappa = \frac{\sum_{m=1}^{M}(v_m - \tilde{v})(r_m - \tilde{r})}{\sqrt{\sum_{m=1}^{M}(v_m - \tilde{v})^2}\sqrt{\sum_{m=1}^{M}(r_m - \tilde{r})^2}}, \tag{4.2}$$

where M denotes the number of samples over the reconstructed and actual ECG signals. v_m and r_m denote the m-th samples over the reconstructed and actual ECG signals, respectively. $\tilde{v}$ and $\tilde{r}$ denote the mean values of the reconstructed and actual ECG signals, respectively. In addition to the correlation coefficient, for the better evaluation of the proposed method, we detected the R-peaks based on the Pan-Tompkins algorithm [87]. This algorithm can detect the R-peak based on an adaptive threshold determined by a signal level. Although it might be possible to detect the R-peak by other algorithms such as the maximum peak detection algorithm, we used the Pan Tompkins algorithm because it can detect the R-peak accurately, according to previous research related to the SCG-based ECG signal reconstruction [45]. Considering that the P peak typically appears within 0.3 s before the R-peak, we thus detected the P peak as the maximum one that appeared within 0.3 s before the R-peak. We finally detected the T peak as the maximum one that appeared after the R-peak. As the performance metric, we calculated the AAE between the timings when such peaks appeared over the reconstructed and actual ECG signals. Precisely, against each peak, the AAE was calculated as

$$AAE = \frac{1}{N}\sum_{n=1}^{N}|t_{\mathrm{pred}}(n) - t_{\mathrm{true}}(n)|, \tag{4.3}$$

where N denotes the number of the collected ECG signals, n means the n th ECG signal, and t_{pred} and t_{true} denote the predicted and ground truth timings, respectively. Furthermore, we measured the P-peak to R-peak interval (PRI), R-peak to T-peak interval (RTI), and P-peak to T-peak interval (PTI), and we calculated the RMSE between these intervals over the reconstructed and actual

ECG signals as

$$RMSE = \sqrt{\frac{1}{N}\sum_{n=1}^{N} |PPI_{\mathrm{pred}}(n) - PPI_{\mathrm{true}}(n)|^2}, \tag{4.4}$$

where PPI_{pred} and PPI_{true} denote the peak intervals measured over the reconstructed and actual ECG signals, respectively.

4.3.3 ECG signal reconstruction accuracy

TABLE 4.2 lists the dataset collected through the experiments. In the evaluation of the experiments, we used the hold-out validation to evaluate our proposed method. The data from one set of subjects were used as the testing data, while the other set of subjects were used as the training data, which was repeated for all the subjects.

Fig. 4.7 shows examples of the reconstructed and actual ECG signals. In these examples, for a better comparison, the amplitudes of these two signals are scaled. From these examples, it can be seen that the ECG signal is reconstructed by our proposed method so that the P, R, and T peaks could be detected. We can also say that detecting the P peak might be difficult, compared to the R and the T peaks. This is because the SNR of the P-wave is low, which makes it challenging to train the proposed deep learning model.

TABLE 4.3 lists the correlation coefficients κ, the AAEs, and the RMSEs of the proposed method. As seen from this table, our proposed method reconstructs the ECG signal with an average correlation coefficient of 0.86. In general, as the HR gets low, one period of the ECG signal grows longer, indicating that our method can reconstruct the ECG signal, regardless of the HR. In terms of the AAE, the average AAEs of the P, R, and T peaks are 28.3 ms, 17.8 ms, and 30.3 ms, respectively. From these results, we can say that our method reconstructs R-peak accurately, compared with the P and T peaks. The SNRs of the P and T-waves are typically lower than that of the R-peak, and the P and T-wave components over the heartbeat signal by the Doppler radar are sensitive to noise, e.g., respiration and body movements. Thus, the AAEs of the P and T peaks are lower than that of the R-peak. When a subject has lower HR, the timing when the T-wave appears tends to be delayed. This fact makes it difficult to reconstruct the T-wave, which could be solved by further extending the diversity of the training data. As a result, the RMSEs of the PRI, RTI,

Table 4.2: Dataset. N denotes the number of the collected heartbeat signals

ID	Sex	Ave. RRI [ms]	Ave. HR [bpm]	N
1	M	886	67.8	192
2	F	887	67.6	184
3	F	818	73.4	192
4	F	837	71.6	188
5	M	1159	51.8	131
6	M	1005	59.7	157
7	M	1043	57.5	144
8	M	1456	41.2	103
9	F	1325	45.3	129

and PTI are 31.6 ms, 33.9 ms, and 47.2 ms, respectively. The required accuracies of the PRI, RTI, and PTI measurements depend on the usage of these intervals. In our future work, we will further improve the ECG signal reconstruction accuracy according to real applications.

4.3.4 Performance comparison of the proposed and existing methods

TABLE 4.4 lists the performance comparison of the proposed and the other existing ECG signal reconstruction methods. The three methods in Table 4 use different datasets and radars, i.e., PPG, SCG, and a Doppler radar. Thus, the performance comparison among these methods is not necessarily fair. However, to show the ability of the proposed non-contact ECG reconstruction method, it would be beneficial to compare our method with the ones that use the contact radars. The method [66] reconstructs the ECG signal by the linear transform of the DCT coefficients of the PPG signal to those of the ECG signal. The SCG-based method [67] reconstructs the ECG signal by associating the SCG signal to the ECG signal through bidirectional-LSTM. From this

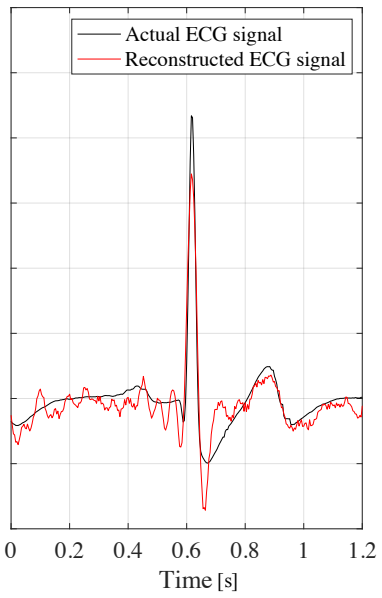

(a) Subject 1.

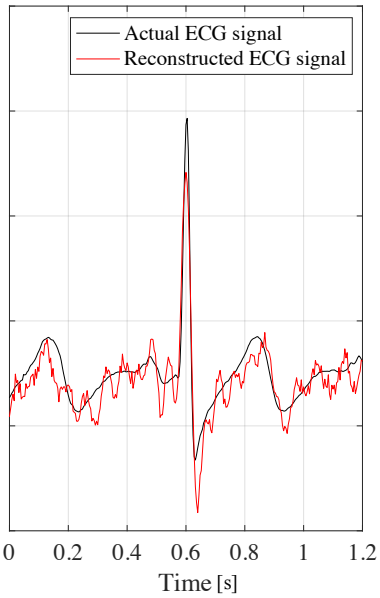

(c) Subject 4.

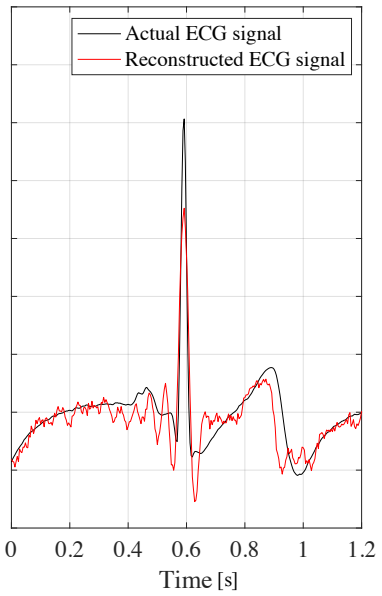

(b) Subject 6.

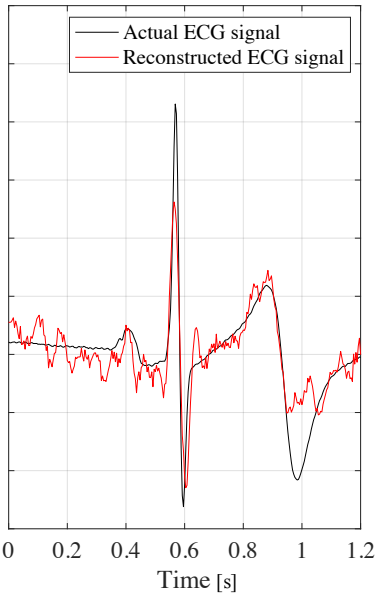

(d) Subject 9.

Figure 4.7: Examples of the reconstructed and actual ECG signals.

Table 4.3: The correlation coefficients κ, the AAEs, and the RMSEs of the proposed method.

ID	Actual Ave. HR [bpm]	κ	AAE [ms]			RMSE [ms]		
			P	R	T	PRI	RTI	PTI
1	67.8	0.91	30.1	13.6	23.6	29.3	36.3	44.2
2	67.6	0.88	27.3	19.8	24.2	33.5	29.8	39.7
3	73.4	0.89	32.5	22.1	27.4	37.7	35.1	42.5
4	71.6	0.89	23.5	17.8	26.2	28.2	32.8	44.9
5	51.8	0.82	36.7	16.7	38.1	35.9	37.1	54.0
6	59.7	0.85	24.4	14.0	29.5	31.3	34.0	49.5
7	57.5	0.81	29.2	19.1	36.2	27.0	30.4	51.7
8	41.2	0.84	23.3	15.8	34.9	29.5	33.5	46.3
9	45.3	0.83	27.8	21.4	33.0	32.0	36.2	52.2
Ave.	-	0.86	28.3	17.8	30.3	31.6	33.9	47.2

table, it can be seen that the PPG-based ECG signal reconstruction method achieves a high correlation coefficient of 0.96, while our proposed method achieves the correlation coefficient of 0.86. Additionally, the AAEs of the P, R, and T peaks by the SCG-based method are 20 ms, 13 ms, and 16 ms, respectively. In contrast, our method's AAEs for the P, R, and T peaks are 28 ms, 17 ms, and 30 ms, respectively. Although the ECG signal reconstruction accuracy of the conventional methods is higher than ours, the experimental results show that our method can reconstruct the ECG signal without device attachment even when a subject is 2.5 m away from a Doppler radar. These results are worth noting, and in our future work, we will try to improve our method to achieve as high an ECG signal reconstruction accuracy as the conventional ones.

Table 4.4: The performance comparison of the proposed and the other existing ECG signal reconstruction methods.

Method	κ	AAE [ms]		
		P	R	T
PPG-based method [66]	0.96	-	-	-
SCG-based method [67]	-	20	13	16
Proposed method	0.86	28	17	30

4.3.5 Limitations of proposed method

Our method might not consistently achieve the good performance of the ECG signal reconstruction, particularly for the types of ECG signal waveforms that are not considered for the model's training. When a subject has a heart disease that can affect the ECG signal waveform, it is necessary to include such a type of ECG signal waveform in the training data. Thus, to make our model further robust to the diversity of the ECG signal waveform, numerous training data are essential. Additionally, our method can be applied after the heartbeat detection. When heartbeat is not detected due to noise such as respiration and body movements, it is impossible to reconstruct the ECG signal. Even when the heartbeat is detected, the performance of the ECG signal reconstruction could be degraded due to the large deformation of the heartbeat signal waveform. This issue could also be solved by increasing the diversity of the training data.

4.4 Conclusion

In this chapter, we present a Doppler radar-based ECG signal reconstruction method by a hybrid deep learning model with CNN and LSTM. As the ECG signal reconstruction method, there exist the ones with the attaching devices, i.e., PPG and SCG. In contrast, to reconstruct an ECG signal

without requiring device attachment, we constructed a deep learning model that outputs the ECG signal by extracting the spatial and temporal features from a heartbeat signal obtained by a Doppler radar. Although detecting the P-wave, the T-wave, and the R-peak with a Doppler radar is more complicated than detecting the only heartbeat due to the low SNR of heartbeat components, we experimentally confirmed that our proposal performed the ECG signal reconstruction well even without device attachment.

Chapter 5

Conclusions and Future Work

5.1 Contributions

This dissertation first proposed the novel heartbeat detection method via a Doppler radar through heartbeat signal reconstruction with deep learning. In contrast to the conventional methods that detect heartbeat by frequency analysis and feature detection, the proposed method introduces noise-robust heartbeat component extraction based on a spectrogram. Our proposed method reconstructs a heartbeat signal from the spectrogram-related data based on deep learning for more accurate heartbeat detection. Through some experiments, we showed our method could perform accurate heartbeat detection even for the long detection range and achieved the small AAE of 3.84 bpm against 17 subjects including 5 subjects with the HR lower than 50 bpm.

Furthermore, we proposed an ECG signal reconstruction method based on deep learning. Conventionally no conventional methods have extracted the P-wave and the T-wave components through a Doppler radar due to the low SNR of heartbeat components, though such components can provide beneficial information on the heart's health condition. In contrast, we introduced ECG signal reconstruction from the Doppler radar-related data by utilizing the advantages of LSTM and CNN. The experimental results showed that the proposed method could reconstruct an ECG signal via a Doppler radar even without device attachment. Through the performance comparison among our proposed and the existing methods with wearable devices, we demonstrated the feasibility of the non-contact ECG signal reconstruction via a Doppler sensor.

5.2 Future Work

Our work could enhance remote sensing systems of cardiac activity via a Doppler radar. In terms of heartbeat detection, we will attempt to apply our method to real applications, such as

- Smart homes that monitor health condition through vital signs
- Burn patient monitoring
- Infant monitoring

To realize these applications, we will still have some problems: (i) a heartbeat signal reconstruction accuracy for large RRI changes, (ii) trustworthiness of heartbeat detection results. On the one hand, when the RRIs change largely, it might be challenging to reconstruct a heartbeat signal accurately. To reconstruct a heartbeat signal for the subject with large RRI changes, it is necessary to train a deep learning model with data including such a case. However, the training data in our method might not be sufficient, and should be more diversified. On the other hand, trustworthiness of heartbeat detection results is very important for real applications, because main action of applications such as anomaly notification is based on the heartbeat detection results. Although the proposed method attempts to detect heartbeat by taking advantage of some signal processing, it is sometimes impossible to detect heartbeat due to large effect of noise and subject's posture. Trustworthiness of heartbeat detection results is quite low in such a case. Thus, we will need to introduce signal quality assessment of a Doppler radar signal for real applications.

Also, we will investigate fetal heartbeat detection via a Doppler ultrasound signal. Conventionally, to realize non-invasive fetal heartbeat monitoring, a Doppler ultrasound-based heartbeat detection method has been extensively studied [88]-[90]. This method could detect fetal heartbeat based on the same principle of a Doppler radar-based heartbeat detection method. However, a Doppler ultrasound signal contains noise related to maternal and fetal motions, which makes it challenging to detect fetal heartbeat with a high accuracy. Thus, we will attempt to realize more accurate fetal heartbeat detection via a Doppler ultrasound signal based on the knowledge on heartbeat detection via a Doppler radar.

Regarding to ECG signal reconstruction, we will need to validate our proposed method based on data with more diversity. Although it might be challenging to evaluate our proposed method

with abnormal ECG data, which is essential for applying our method to real applications. The evolve of deep learning probably leads to further improvement of cardiac sensing technology.

References

[1] R. E. Kleiger, P. K. Stein, and J. T. Bigger Jr, "Heart rate variability: measurement and clinical utility," *A*nnals of Noninvasive Electrocardiology, vol. 10, pp. 88-101, Jan. 2005.

[2] J. Allen, "Photoplethysmography and its application in clinical physiological measurement," *Physiological Measurement*, vol. 28, no. 3, pp. R1-R39, Feb. 2007.

[3] C. Li, V. M. Lubecke, O. Boric-Lubecke, and J. Lin, "A review on recent advances in Doppler radar sensors for noncontact healthcare monitoring," *IEEE Transactions on Microwave Theory and Techniques*, vol. 61, pp. 2046-2060, May. 2013.

[4] A. F. Hussein, M. Burbano-Fernandez, G. Ramirez-Gonzalez, E. Abdulhay, and V. H. C. De Albuquerque, "An automated remote cloud-based heart rate variability monitoring system," *IEEE Access*, vol. 6, pp. 77055-77064, 2018.

[5] D. Mocrii, Y. Chen, and P. Musilek, "IoT-based smart homes: A review of system architecture, software, communications, privacy and security," *Internet of Things*, vol. 1, pp. 81-98, 2018.

[6] H. Jiang, C. Cai, X. Ma, Y. Yang, and J. Liu, "Smart home based on WiFi sensing: A survey," *IEEE Access*, vol. 6, pp. 13317-13325, 2018.

[7] P. J. Schwartz, and M. J. Ackerman, "The long QT syndrome: a transatlantic clinical approach to diagnosis and therapy," *European Heart Journal*, vol. 34, pp. 3109-3116, 2013.

[8] P. E. Lazzerini, P. L. Capecchi, and F. Laghi-Pasini,"Long QT syndrome: an emerging role for inflammation and immunity," *Frontiers in Cardiovascular Medicine*, vol. 26, Feb. 2015.

[9] H. Turhan, E. Yetkin, R. Atak, T. Altinok, K. Senen, M. Ileri, and E. Kutuk, "Increased P ‐ wave duration and P ‐ wave dispersion in patients with aortic stenosis," *Annals of Noninvasive Electrocardiology*, vol. 8, 18-21, Jan. 2003.

[10] C. Gu, C. Li, J. Lin, J. Long, J. Huangfu, AND L. Ran, "Instrument-based noncontact Doppler radar vital sign detection system using heterodyne digital quadrature demodulation architecture," *IEEE Transactions on Instrumentation and Measurement*, vol. 59, no. 6, pp. 1580-1588, June 2010.

[11] G. Vinci, S. Lindner, F. Barbon, S. Mann, M. Hofmann, A. Duda, and A. Koelpin, "Six-port radar sensor for remote respiration rate and heartbeat vital-sign monitoring," *IEEE Transactions on Microwave Theory and Techniques*, vol. 61, no. 5, pp. 2093-2100, May 2013.

[12] I. Guler, F. Hardalac, and N. Barisci, "Application of FFT analyzed cardiac Doppler signals to fuzzy algorithm," *Computers in biology and medicine*, vol. 32, pp. 435-444, 2002.

[13] J. Tu and J. Lin, "Respiration harmonics cancellation for accurate heart rate measurement in non-contact vital sign detection," *IEEE MTT-S International Microwave Symposium Digest (MTT)*, Jun. 2013, pp. 1-3.

[14] J. Tu and J. Lin, "Fast acquisition of heart rate in noncontact vital sign radar measurement using time-window-variation technique," *IIEEE Transactions on Instrumentation and Measurement*, vol. 65, pp. 112-122, Jan. 2016.

[15] A. Tariq and H. G. Shiraz, "Doppler radar vital signs monitoring using wavelet transform," *Loughborough Antennas and Propagation Conference*, pp. 293-296, Nov. 2010.

[16] M. Sekine and K. Maeno, "Non-contact heart rate detection using periodic variation in Doppler frequency," in *Proc. IEEE Sensors Application Symposium*, pp. 318-322, Feb. 2011.

[17] A. Tariq and H. G. Shiraz, "Vital signs detection using Doppler radar and continuous wavelet transform," *IEEE European Conference on Antennas and Propagation (EUCAP)*, pp. 285-288, Apr. 2015

[18] M. He, Y. Nian, and B. Liu, "Noncontact heart beat signal extraction based on wavelet transform," *IEEE International Conference on Biomedical Engineering and Informatics (BMEI)*, pp. 209-213, Oct. 2015.

[19] M. Li and J. Lin, "Wavelet-Transform-Based Data-Length-Variation Technique for Fast Heart Rate Detection Using 5.8-GHz CW Doppler Radar," *IEEE Transactions on Microwave Theory and Techniques*, vol. 66, pp. 568-576, Jan. 2018.

[20] P. Bechet, R. Mitran, and M. Munteanu, "A non-contact method based on multiple signal classification algorithm to reduce the measurement time for accurately heart rate detection," *Review of Scientific Instruments*, vol. 84, Aug. 2013.

[21] K. J. Lee, C. Park, and B. Lee, "Tracking driver's heart rate by continuous-wave Doppler radar," *IEEE Engineering in Medicine and Biology Society (EMBC)*, pp. 5417-5420, Aug. 2016.

[22] K. Yamamoto, K. Toyoda, and T. Ohtsuki, "Non-contact Heartbeat Detection by MUSIC with Discrete Cosine Transform-based Parameter Adjustment," *IEEE Global Communications Conference (GLOBECOM)*, pp. 1-6, Dec. 2018.

[23] K. Yamamoto, K. Toyoda, and T. Ohtsuki, "MUSIC-based Non-contact Heart Rate Estimation with Adaptive Window Size Setting," *IEEE Engineering in Medicine and Biology Society (EMBC)*, pp. 6073-6076July. 2019.

[24] J. Park, J. W. Ham, S. Park, D. H. Kim, S. J. Park, H. Kang, and S. O. Park, "Polyphase-basis discrete cosine transform for real-time measurement of heart rate with CW Doppler radar," *IEEE Transactions on Microwave Theory and Techniques*, vol. 66, pp. 1644-1659, Mar. 2017.

[25] M. Nosrati and N. Tavassolian, "High-accuracy heart rate variability monitoring using Doppler radar based on Gaussian pulse train modeling and FTPR algorithm," *IEEE Transactions on Microwave Theory and Techniques*, vol. 66, pp. 556-567, Jan. 2017.

[26] C. Will, K. Shi, F. Lurz, R. Weigel, and A. Koelpin, "Instantaneous heartbeat detection using a cross-correlation based template matching for continuous wave radar systems," *IEEE Topical Conference on Wireless Sensors and Sensor Networks (WiSNet)*, Jan. 2016.

[27] C. Will, K. Shi, R. Weigel, and A. Koelpin, "Advanced template matching algorithm for instantaneous heartbeat detection using continuous wave radar systems," *IEEE MTT-S International Microwave Bio Conference (IMBIOC)*, pp. 1-4, May 2017.

[28] S. Bounyong, M. Yoshioka, and J. Ozawa, "Monitoring of a driver's heart rate using a microwave sensor and template-matching algorithm," *IEEE International Conference on Consumer Electronics (ICCE)* pp. 43-44, Jan. 2017.

[29] S. Izumi, T. Okano, D. Matsunaga, H. Kawaguchi, and M. Yoshimoto, "Non-contact instantaneous heart rate extraction system using 24-GHz microwave Doppler sensor," *IEICE Transactions on Communications*, 2018.

[30] I. V. Mikhelson, P. Lee, S. Bakhtiari, T. W. Elmer, A. K. Katsaggelos, and A. V. Sahakian, "Noncontact millimeter-wave real-time detection and tracking of heart rate on an ambulatory subject," *IEEE Transactions on Information Technology in Biomedicine*, vol. 16, no. 5, pp. 927-934, Sep. 2012.

[31] T. Ohtsuki and E. Mogi, "Heartbeat detection with Doppler radar based on estimation of average RR interval using Viterbi algorithm," *IEEE International Symposium on Personal, Indoor, and Mobile Radio Communications (PIMRC)*, pp. 1-5, Sep. 2016.

[32] X. Yang, G. Sun, and K. Ishibashi, "Non-contact acquisition of respiration and heart rates using doppler radar with time domain peak-detection algorithm," *IEEE International Conference of Engineering in Medicine and Biology Society (EMBC)*, pp. 2847-2850, July 2017.

[33] J. Y. Kim, J. H. Park, S. Y. Jang,and J. R. Yang, "Peak detection algorithm for vital sign detection using Doppler radar sensors," *Sensors*, vol. 19, Jan. 2019.

[34] R. Hiromatsu, K. Yamamoto, K. Toyoda, and T. Ohtsuki, "Novel CA-CFAR approach for improvement of doppler sensor-based heart rate variability estimation," *IEEE International*

Conference of Engineering in Medicine and Biology Society (EMBC) pp. 796-799, July 2019.

[35] K. Yamamoto and T. Ohtsuki, "Noncontact Heartbeat Detection by Viterbi Algorithm with Fusion of Beat-Beat Interval and Deep Learning-Driven Branch Metrics," *IEEE International Conference on Acoustics, Speech and Signal Processing (ICASSP)* pp. 8308-8312, June 2021.

[36] S. Tomii and T. Ohtsuki, "Heartbeat detection by using Doppler radar with wavelet transform based on scale factor learning," *IEEE International Conference on Communications (ICC)*, pp. 483-488, Jun. 2015.

[37] E. Mogi and T. Ohtsuki, "Heartbeat detection with Doppler sensor using adaptive scale factor selection on learning," *IEEE International Symposium on Personal, Indoor, and Mobile Radio Communications (PIMRC)*, pp. 2166-2170, Aug. 2015.

[38] J. Saluja, J.Casanova, and J. Lin, "A supervised machine learning algorithm for heart-rate detection using doppler motion-sensing radar," *IEEE Journal of Electromagnetics, RF and Microwaves in Medicine and Biology*, vol. 4, pp. 45-51, 2019.

[39] Y. Iwata, H. T. Thanh, G. Sun, and K. Ishibashi, "High Accuracy Heartbeat Detection from CW-Doppler Radar Using Singular Value Decomposition and Matched Filter," *Sensors*, vol. 21, 2021.

[40] T. Sakamoto, R. Imasaka, H. Taki, T. Sato, M. Yoshioka, K. Inoue, and H. Sakai, "Feature-based correlation and topological similarity for interbeat interval estimation using ultrawideband radar," *IEEE Transactions on Biomedical Engineering*, vol. 63, pp. 747-757. Apr. 2016.

[41] W. Hu , Z. Zhao, Y. Wang, H. Zhang, and F. Lin, "Noncontact accurate measurement of cardiopulmonary activity using a compact quadrature Doppler radar sensor," *IEEE Transactions on Biomedical Engineering*, vol. 61, no. 3, pp. 725-735, Mar. 2014.

[42] V. L. Petrovic, M. M. Jankovic, A. V. Lupsic, V. R. Mihajlovic, and J. S. Popovic-Bozovic, "High-accuracy real-time monitoring of heart rate variability using 24 GHz continuous-wave Doppler radar" *IEEE Access*, vol. 7, pp. 74721-74733, 2019.

[43] K. Yamamoto, K. Toyoda, and T. Ohtsuki,"Spectrogram-based Non-contact RRI Estimation by Accurate Peak Detection Algorithm," *IEEE Access*, vol. 6, pp. 60369-60379, Oct. 2018.

[44] A. D. Droitcour, O. Boric-Lubecke, and G, T. Kovacs, "Signal-to-noise ratio in Doppler radar system for heart and respiratory rate measurements. IEEE Transactions on Microwave Theory and Techniques", vol. 57, pp. 2498-2507, Oct. 2009.

[45] Y. S. Lee, P. N. Pathirana, C. L. Steinfort, and T. Caelli, "Monitoring and analysis of respiratory patterns using microwave doppler radar," *IEEE Journal of Translational Engineering in Health and Medicine*, vol. 2, pp. 1-12, Feb. 2014.

[46] N. T. P. Van, L. Tang, A. Singh, N. D. Minh, S. C. Mukhopadhyay, and S. F. Hasan, Self-identification respiratory disorder based on continuous wave radar sensor system. *IEEE Access*, vol. 7, pp. 40019-40026, 2019.

[47] H. Zhao, H. Hong, D. Miao, Y. Li, H. Zhang, Y. Zhang, and X. Zhu, X, "A noncontact breathing disorder recognition system using 2.4-GHz digital-IF Doppler radar," *IEEE Journal of Biomedical and Health Informatics*, vol. 23, pp. 208-217, Jan. 2018.

[48] B. Y. Su, and K. C. Ho, M. ZJ. Rantz, and M. Skubic, "Doppler radar fall activity detection using the wavelet transform," *IEEE Transactions on Biomedical Engineering*, vol. 62, pp. 865-875, Mar. 2015.

[49] M. G. Amin, Y. D. Zhang, F. Ahmad,, and K. D. Ho, "Radar signal processing for elderly fall detection: The future for in-home monitoring," *IEEE Signal Processing Magazine*, vol. 33, pp. 71-80, Feb. 2016.

[50] S. Z. Gurbuz and M. G. Amin, "Radar-based human-motion recognition with deep learning: Promising applications for indoor monitoring," *IEEE Signal Processing Magazine*, vol. 36, pp. 16-28, Apr. 2019.

[51] B. F Wu, P. W Huang, T. Y. Tsou, T. M. Lin, and M. L. Chung, "Camera-based heart rate measurement using continuous wavelet transform," *IEEE International Conference on System Science and Engineering (ICSSE)*, pp. 7-11, July 2017.

[52] B. A. Sujathakumari, B. S. Shreeharsha, P. Verma, S. Shivram, and A. R. Raksha, "Heart Rate Measurement using Face Video with Noise Suppression," *International Conference for Convergence in Technology*, pp. 1-7, Oct. 2018.

[53] G. Bai, J. Huang, and H. Liu, "Real-time robust noncontact heart rate monitoring with a camera," *IEEE Access*, vol. 6, pp. 33682-33691, 2018

[54] Q. Chen, X. Jiang, X. Liu, C. Lu, L Wang, and W. Chen, "Non-Contact Heart Rate Monitoring in Neonatal Intensive Care Unit using RGB Camera," *IEEE International Conference of Engineering in Medicine and Biology Society (EMBC)*, pp. 5822-5825, July 2020.

[55] M. Simjanoska, M. Gjoreski, M. Gams, and A. Madevska Bogdanova, "Non-invasive blood pressure estimation from ECG using machine learning techniques," *Sensors*, vol. 18, Jan. 2018.

[56] C. Landry, S. D. Peterson, and A. Arami, "Estimation of the Blood Pressure Waveform using Electrocardiography," *IEEE International Conference of Engineering in Medicine and Biology Society (EMBC)* pp. 7060-7063, July 2019.

[57] F. Miao, B. Wen, Z. Hu, G. Fortino, X. P. Wang, Z. D. Liu, and Y. Li, "Continuous blood pressure measurement from one-channel electrocardiogram signal using deep-learning techniques," *Artificial Intelligence in Medicine*, vol. 108, Aug. 2020.

[58] Y. Liang, Z. Chen, R. Ward, and M. Elgendi, "Photoplethysmography and deep learning: enhancing hypertension risk stratification," *Biosensors*, vol. 8, Oct. 2018.

[59] O. Schlesinger, N. Vigderhouse, D. Eytan, and Y. Moshe, "Blood pressure estimation from ppg signals using convolutional neural networks and siamese network," *IEEE International Conference on Acoustics, Speech and Signal Processing (ICASSP)*, pp. 1135-1139, May 2020.

[60] M. Kachuee, M. M. Kiani, H. Mohammadzade, and M. Shabany, "Cuffless blood pressure estimation algorithms for continuous health-care monitoring," *IEEE Transactions on Biomedical Engineering*, vol. 64, pp. 859-869, June 2016.

[61] Q. Zhang, X. Zeng, W. Hu, and D. Zhou, "A machine learning-empowered system for long-term motion-tolerant wearable monitoring of blood pressure and heart rate with ear-ECG/PPG," *IEEE Access*, vol. 5, pp. 10547-10561, May 2017.

[62] C. Landry, S. D. Peterson, and A. Arami, "Nonlinear dynamic modeling of blood pressure waveform: Towards an accurate cuffless monitoring system," *IEEE Sensors Journal*, vol. 20, pp. 5368-5378, Jan. 2020.

[63] T. Ohata, K. Ishibashi, and G. Sun, "Non-Contact Blood Pressure Measurement Scheme Using Doppler Radar," *IEEE International Conference of Engineering in Medicine and Biology Society (EMBC)*, pp. 778-781, July 2019.

[64] H. Zhao, X. Gu, H. Hong, Y. Li, X. Zhu and C. Li, "Non-contact Beat- to-beat Blood Pressure Measurement Using Continuous Wave Doppler Radar," *IEEE/MTT-S International Microwave Symposium*, pp. 1413-1415, June 2018.

[65] S. Ishizaka, K. Yamamoto, and T. Ohtsuki, "Non-contact Blood Pressure Measurement using Doppler Radar based on Waveform Analysis by LSTM," *IEEE International Conference on Communications (ICC)*, June 2021.

[66] Q. Zhu, X. Tian, C. W. Wong, and M. Wu, "Learning Your Heart Actions From Pulse: ECG Waveform Reconstruction From PPG," *bioRxiv*, 815258, 2019.

[67] J. Park, H. Cho, W. Hwang, R. K. Balan, and J. Ko, "Deep ECG Wave Estimation Model with Seismograph Sensor," *ACM International Conference on Mobile Systems, Applications, and Services (MobiSys)*, pp. 568-569, June 2019.

[68] S. H. I. Xingjian, Z. Chen, H. Wang, D. Y. Yeung, W. K. Wong, and W. C. Woo, "Convolutional LSTM network: A machine learning approach for precipitation nowcasting," *Advances in Neural Information Processing Systems*, pp. 802-810, 2015.

[69] S. Hochreiter and J. Schmidhuber, "Long Short-Term Memory," *Neural Computation*, vol. 9, no. 8, pp. 1735-1780, 1997.

[70] O. Yildirim, "A novel wavelet sequence based on deep bidirectional LSTM network model for ECG signal classification," *Computers in Biology and Medicine*, vol. 96, pp. 189-202, 2018.

[71] P. Wang, A. Jiang, X. Liu, J. Shang, and L. Zhang, "LSTM-based EEG classification in motor imagery tasks," *IEEE Transactions on Neural Systems and Rehabilitation Engineering*, vol. 26, pp. 2086-2095, Nov. 2018.

[72] R. Wang, X. Liang, X. Zhu, and Y. Xie, "A feasibility of respiration prediction based on deep Bi-LSTM for real-time tumor tracking," *IEEE Access*, vol. 6, pp. 51262-51268, 2018.

[73] S. Lawrence, C. L. Giles, A. C. Tsoi, and A. D. Back, "Face recognition: A convolutional neural-network approach," *IEEE Transactions on Neural Networks*, vol. 8, 98-113, Jan. 1997.

[74] O. Ronneberger, P. Fischer, and T. Brox, "U-net: Convolutional networks for biomedical image segmentation," Springer Medical Image Computing and Computer-assisted Intervention, pp. 234-241, Oct. 2015.

[75] K. He, X. Zhang, S. Ren, and J. Sun, "Deep residual learning for image recognition," *IEEE Computer Vision and Pattern Recognition*, pp. 770-778, 2016.

[76] S. Kiranyaz, T. Ince, and M. Gabbouj, "Real-time patient-specific ECG classification by 1-D convolutional neural networks," *IEEE Transactions on Biomedical Engineering*, vol. 63, pp. 664-675, Mar. 2015.

[77] N. Ballas, L. Yao, C. Pal, and A. Courville, "Delving deeper into convolutional networks for learning video representations," *arXiv*, 2016.

[78] S. Sudhakaran and O. Lanz, "Learning to detect violent videos using convolutional long short-term memory," *IEEE International Conference on Advanced Video and Signal Based Surveillance (AVSS)*, pp. 1-6, Aug. 2017.

[79] L. Zhang, G. Zhu, L. Mei, P. Shen, S. A. A. Shah, and M. Bennamoun, "Attention in convolutional LSTM for gesture recognition," *Advances in Neural Information Processing Systems*, pp. 1953-1962, 2018.

[80] Z. Zhang, Z. Pi, and B. Liu, "TROIKA: A general framework for heart rate monitoring using wrist-type photoplethysmographic signals during intensive physical exercise," *IEEE Transactions on Biomedical Engineering*, vol. 62, pp. 522-531, Feb. 2014.

[81] R. W. Wijshoff, M. Mischi, and R. M. Aarts, "Reduction of periodic motion artifacts in photoplethysmography," *IEEE Transactions on Biomedical Engineering*, vol. 64, pp., 196-207, Jan. 2016.

[82] A. Temko, "Accurate heart rate monitoring during physical exercises using PPG," *IEEE Transactions on Biomedical Engineering*, vol. 64, pp. 2016-2024, Sep. 2017.

[83] M. A. Garcia-Gonzalez, A. Argelagos-Palau, M. Fernandez-Chimeno, and J. Ramos-Castro, "A comparison of heartbeat detectors for the seismocardiogram," *IEEE Computing in Cardiology* pp. 461-464, Sep. 2013.

[84] Y. Li, X. Tang, and Z. Xu, "An approach of heartbeat segmentation in seismocardiogram by matched-filtering," *Int. Proc. IEEE Intelligent Human-machine Systems and Cybernetics* vol. 2, pp. 47-51, Aug. 2015.

[85] T. Choudhary, L. M. Sharma, and M. K. Bhuyan, "Standalone heartbeat extraction in SCG signal using variational mode decomposition,". *IEEE International Conference on Wireless Communications, Signal Processing and Networking (WiSPNET)*, pp. 1-4, Mar. 2018.

[86] M. Nosrati and N. Tavassolian, "Accurate Doppler radar-based cardiopulmonary sensing using chest-wall acceleration," *IEEE Journal of Electromagnetics, RF and Microwaves in Medicine and Biology*, vol. 3, pp. 41-47, Jan. 2018.

[87] J. Pan and W. J. Tompkins, "A real-time QRS detection algorithm," *IEEE Transactions on Biomedical Engineering*, pp. 230-236., March 1985.

[88] J. Jezewski, D. Roj, J. Wrobel, and K. Horoba, "A novel technique for fetal heart rate estimation from Doppler ultrasound signal," *Biomedical engineering online*, vol. 10, pp. 1-17, 2011.

[89] A. B. Queyam, S. K. Pahuja, and D. Singh, "Doppler ultrasound based non-invasive heart rate telemonitoring system for wellbeing assessment. International Journal of Intelligent Systems and Applications", vol. 11, 2018.

[90] P. Hamelmann, R. Vullings, A. F. Kolen, J. W. Bergmans, J. O. van Laar, P. Tortoli, and M. Mischi, "Doppler ultrasound technology for fetal heart rate monitoring: a review," *IEEE Transactions on Ultrasonics, Ferroelectrics, and Frequency Control*, vol. 67, pp. 226-238, 2019.

Appendix A

List of Author's Publications and Awards

A.1 Journals

1. K. Yamamoto and T. Ohtsuki, "ECG Signal Reconstruction via Doppler Sensor by Hybrid Deep Learning Model with CNN and LSTM," *IEEE Access*, vol. 8, pp. 130551-130560, July 2020.

2. K. Yamamoto and T. Ohtsuki, "Non-contact Heartbeat Detection by Heartbeat Signal Reconstruction based on Spectrogram Analysis with Convolutional LSTM," *IEEE Access*, vol. 8, pp. 123603-123613, June 2020.

3. K. Yamamoto, K. Toyoda, and T. Ohtsuki, "Doppler Sensor-based Blink Duration Estimation by Analysis of Eyelids Closing and Opening Behavior on Spectrogram," *IEEE Access*, vol. 7, pp. 42726-42734, Mar. 2019.

4. K. Yamamoto, K. Toyoda, and T. Ohtsuki, "Spectrogram-based Non-contact RRI Estimation by Accurate Peak Detection Algorithm," *IEEE Access*, vol. 6, pp. 60369-60379, Oct. 2018.

A.2 Full Articles on International Conferences Proceedings

1. S. Ishizaka, K. Yamamoto, and T. Ohtsuki, "Non-contact Blood Pressure Measurement using Doppler Radar based on Waveform Analysis by LSTM," *IEEE International Conference on Communications (ICC)*, Montreal, Canada, June 2021.

2. K. Yamamoto and T. Ohtsuki, "Noncontact Heartbeat Detection by Viterbi Algorithm with Fusion of Beat-Beat Interval and Deep Learning-driven Branch Metrics," *IEEE International Conference on Acoustics, Speech and Signal Processing (ICASSP)*, Toronto, Canada, June 2021.

3. T. Nakamura, B. Mondher, K. Yamamoto, and T. Ohtsuki, "Wi-Fi-CSI-based Fall Detection by Spectrogram Analysis with CNN," IEEE Global Communications Conference (GLOBECOM), Taipei, Taiwan, Dec. 2020.

4. K. Tsuchiya, K. Mochizuki, T. Ohtsuki, T. and K. Yamamoto, "Heartbeat Detection Technology for Monitoring Driver's Physical Condition," *SAE Technical Paper*, Detroit, USA, Apr. 2020.

5. K. Yamamoto, K. Toyoda, and T. Ohtsuki, "CNN-based Respiration Rate Estimation in Indoor Environments via MIMO FMCW Radar," *IEEE Global Communications Conference (GLOBECOM)*, Waikoloa, Hawaii, USA, Dec. 2019.

6. W. Takabatake, K. Yamamoto, K. Toyoda, T. Ohtsuki, Y. Shibata, and A. Nagate, "FMCW Radar-based Anomaly Detection in Toilet by Supervised Machine Learning Classifier," *IEEE Global Communications Conference (GLOBECOM)*, Waikoloa, Hawaii, USA, Dec. 2019.

7. K. Yamamoto, K. Toyoda, and T. Ohtsuki, "MUSIC-based Non-contact Heart Rate Estimation with Adaptive Window Size Setting," *IEEE Engineering in Medicine and Biology Society (EMBC)*, Berlin, Germany, July 2019.

8. R. Hiromatsu, K. Yamamoto, K. Toyoda, and T. Ohtsuki, "Novel CA-CFAR Approach for Improvement of Doppler Sensor-based Heart Rate Variability Estimation," *IEEE Engineering in Medicine and Biology Society (EMBC)*, Berlin, Germany, July 2019.

9. K. Yamamoto, K. Toyoda, and T. Ohtsuki, “Spectrogram-based Simultaneous Heartbeat and Blink Detection Using Doppler Sensor,” *IEEE International Conference on Communications (ICC)*, Shanghai, China, May 2019.

10. K. Yamamoto, K. Toyoda, and T. Ohtsuki, “Non-Contact Heartbeat Detection by MUSIC with Discrete Cosine Transform-Based Parameter Adjustment,” *IEEE Global Communications Conference (GLOBECOM)*, Abu Dhabi, United Arab Emirates, Dec. 2018.

11. K. Yamamoto, K. Toyoda, and T. Ohtsuki, “Doppler Sensor-based Blink Duration Estimation by Spectrogram Analysis,” *IEEE International Conference on Communications (ICC)*, Kansas City, USA, May 2018.

12. K. Yamamoto, K. Toyoda, and T. Ohtsuki, “Driver’s Blink Detection Using Doppler Sensor, ” *IEEE International Symposium on Personal, Indoor and Mobile Radio Communications (PIMRC)*, Montreal, Canada, Oct. 2017.

A.3 Domestic Conference Proceedings

1. 石坂秀壮，山本幸平, 大槻知明, “LSTM による波形解析に基づくドップラーレーダを用いた非接触血圧測定, ”電子情報通信学会ヘルスケア・医療情報通信技術研究会（MICT），オンライン開催，2020 年 11 月 4 日発表済み.

2. 廣松亮祐, 山本幸平, 大槻知明, “Bi-LSTM を用いたドップラーセンサ受信信号からの ECG 信号波形復元, ”電子情報通信学会無線通信システム研究会（RCS）, 東京工業大学, 2020 年 3 月 4 日 (会議中止).

3. 高畠航, B. Mondher, 山本幸平, 大槻知明, 柴田洋平, 長手厚史, “LSTM によるスペクトログラム解析に基づく FMCW レーダを用いたトイレ内異常検知, ”電子情報通信学会無線通信システム研究会（RCS）, 東京工業大学, 2020 年 3 月 4 日 (会議中止).

4. 中村崇志, B. Mondher, 山本幸平, 大槻知明, “チャネル状態情報のスペクトログラム画像に基づく部屋に依存しない転倒検知, ”電子情報通信学会無線通信システム研究会（RCS）, 広島市青少年センター, 2020 年 1 月 23 日発表済み.

5. 山本幸平, 豊田健太郎, 大槻知明,“ MIMO FMCW レーダを用いた CNN に基づく呼吸検出,”電子情報通信学会ソサイエティ大会, 大阪大学, 2019 年 9 月 12 日発表済み.

6. 山本幸平, 豊田健太郎, 大槻知明,“ ドップラーセンサを用いたスペクトログラムに基づく心拍および瞬きの同時検出,”電子情報通信学会センサネットワークとモバイルインテリジェンス研究会（SeMI）, 大阪府立大学 I-Site なんば, 2019 年 7 月 12 日発表済み.

7. 高畠航, 山本幸平, 豊田健太郎, 大槻知明, 柴田洋平, 長手厚史,“ プライバシを考慮した FMCW レーダを用いたトイレ内異常検知,”電子情報通信学会総合大会, 早稲田大学, 2019 年 3 月 20 日発表済み.

8. 山本幸平, 豊田健太郎, 大槻知明,“ スペクトログラムに基づく非接触型心拍検出法の精度改善,”電子情報通信学会総合大会, 早稲田大学, 2019 年 3 月 19 日発表済み.

9. 廣松亮祐, 山本幸平, 豊田健太郎, 大槻知明,“ ドップラーセンサを用いた心拍推定時の適応ガードセル長を適用した CA-CFAR による体動起因雑音低減,”電子情報通信学会総合大会, 早稲田大学, 2019 年 3 月 19 日発表済み.

10. Win Thu Zar, K. Yamamoto, and T. Ohtsuki,“Spectrogram-based Noncontact RRI Estimation with Viterbi Algorithm,”電子情報通信学会総合大会, 早稲田大学, 2019 年 3 月 19 日発表済み.

11. 山本幸平, 豊田健太郎, 大槻知明,“ [招待講演] Globecom2018 における e-Health 及び smart Home に関する研究動向,”電子情報通信学会モバイルネットワークとアプリケーション研究会（MoNA）, 東京大学, 2019 年 3 月 5 日発表済み.

12. 山本幸平, 豊田健太郎, 大槻知明,“ ドップラーセンサを用いた MUSIC アルゴリズムに基づく心拍数推定,”電子情報通信学会知的環境とセンサネットワーク研究会（ASN）, 指宿, 2019 年 1 月 29 日発表済み.

13. 高畠航, 山本幸平, 豊田健太郎, 大槻知明, 柴田洋平, 長手厚史,“ FMCW レーダを用いたトイレでの異常検知,”電子情報通信学会知的環境とセンサネットワーク研究会（ASN）, 指宿, 2019 年 1 月 29 日発表済み.

14. 廣松亮祐, 豊田健太郎, 大槻知明, 山本幸平, ”ドップラーセンサを用いた心拍推定時のCA-CFAR による体動起因の雑音低減,” 電子情報通信学会知的環境とセンサネットワーク研究会（ASN）, 東京電機大学, 2018 年 11 月 6 日発表済み.

15. 山本幸平, 豊田健太郎, 大槻知明,“MUSIC アルゴリズムに基づく非接触型心拍数推定,” 電子情報通信学会ソサイエティ大会, 金沢大学, 2018 年 9 月 13 日発表済み.

16. 山本幸平, 豊田健太郎, 大槻知明,“ 体動に起因する雑音の影響を考慮したドップラーセンサを用いた瞬き検出, ” 電子情報通信学会知的環境とセンサネットワーク研究会（ASN）, 鶴岡市先端研究産業支援センター, 2017 年 11 月 17 日発表済み.

17. 山本幸平, 豊田健太郎, 大槻知明,“ 体動に起因する雑音の影響を考慮したドップラーセンサを用いた瞬き検出,” 電子情報通信学会ソサイエティ大会, 東京都市大学, 2017 年 9 月 14 日発表済み.

18. 山本幸平, 豊田健太郎, 大槻知明,“ ドップラーセンサを用いた瞬き長推定に関する一検討, ”電子情報通信学会知的環境とセンサネットワーク研究会（ASN）, 北海道大学, 2017 年 7 月 21 日発表済み.

A.4 Patents

1. 大槻知明, 山本幸平, 北川月子, 生体情報検出システム・プログラム・生体情報検出方法, 出願番号 2021-093563, 2021 年 2 月 18 日出願

2. 大槻知明, 山本幸平, 呼吸検出システム・呼吸検出方法, 出願番号 PCT/JP2020/031523, 2020 年 8 月 20 日出願

3. 大槻知明, 山本幸平, 生体検出装置・生体検出方法・プログラム, 出願番号 2020-140401, 2020 年 8 月 21 日出願

4. 大槻知明, 廣松亮祐, 山本幸平, 石坂秀壮, AI を用いた信号復元システム・信号復元方法・プログラム・信号生成システム, 出願番号 2020-028681, 2020 年 2 月 21 日出願

5. 大槻知明, 山本幸平, 呼吸検出システム・呼吸検出方法, 出願番号 2019-152755, 2019 年 8 月 23 日出願

6. 大槻知明, 山本幸平, 瞬き検出システム・瞬き検出方法, 出願番号 2017-154272, 2017 年 8 月 9 日出願.

A.5 Awards

1. 山本幸平, 優秀発表賞，電子情報通信学会モバイルネットワークとアプリケーション研究会, 2019 年 4 月選定, 2019 年 7 月授賞式.

2. 山本幸平, 若手研究奨励賞，電子情報通信学会知的環境とセンサネットワーク研究会, 2017 年 4 月選定,2018 年 5 月授賞式.